

# The Dance of Heating and Cooling in Galaxy Clusters: 3D Simulations of Self-Regulated AGN Outflows

M. Gaspari<sup>1\*</sup>, C. Melioli<sup>1</sup>, F. Brighenti<sup>1</sup>, A. D’Ercole<sup>2</sup>

<sup>1</sup>*Astronomy Department, University of Bologna, Via Ranzani 1, 40127 Bologna, Italy*

<sup>2</sup>*INAF-OABO, Via Ranzani 1, 40127 Bologna, Italy*

## ABSTRACT

It is now widely accepted that heating processes play a fundamental role in galaxy clusters, struggling in an intricate but fascinating ‘dance’ with its antagonist, radiative cooling. Last generation observations, especially X-ray, are giving us tiny hints about the notes of this endless ballet. Cavities, shocks, turbulence and wide absorption-lines indicate the central active nucleus is injecting huge amount of energy in the intracluster medium. However, which is the real dominant engine of self-regulated heating?

One of the model we propose are massive subrelativistic outflows, probably generated by a wind disc or just the result of the entrainment on kpc scale by the fast radio jet. Using a modified version of AMR code FLASH 3.2, we explored several feedback mechanisms which self-regulate the mechanical power. Two are the best schemes that answer our primary question, id est quenching cooling flow and at the same time preserving a cool core appearance for a long term evolution (7 Gyr): one more explosive (with efficiencies  $\sim 5 \times 10^{-3} - 10^{-2}$ ), triggered by central cooled gas, and the other gentler, ignited by hot gas Bondi accretion (with  $\epsilon = 0.1$ ). These three-dimensional simulations show that the total energy injected is not the key aspect, but the results strongly depend on how energy is given to the ICM. We follow the dynamics of best models (temperature, density, SB maps and profiles) and produce many observable predictions: buoyant bubbles, ripples, turbulence, iron abundance maps and hydrostatic equilibrium deviation. We present a deep discussion of merits and flaws of all our models, with a critical eye towards observational concordance.

**Key words:** cooling flows – galaxies: active – galaxies: jets – hydrodynamics – X-rays: galaxies: clusters

## 1 INTRODUCTION

A fundamental gap in our understanding of the formation and evolution of galaxies and galaxy clusters concerns the thermal evolution of the baryonic component of these systems (e.g. McNamara & Nulsen 2007 [MN07]; Cattaneo et al. 2009). Massive dark matter halos contain large amount of hot gas, shining in the X-ray band. The observed radiative losses, if not compensated for by some kind of heating, would imply gas cooling rates ranging from  $\sim 1 M_{\odot} \text{ yr}^{-1}$ , for massive elliptical galaxies, to hundreds  $M_{\odot} \text{ yr}^{-1}$  for rich clusters (Fabian 1994; Peres et al. 1998). However, since the first XMM-RGS observations it has been clear that the (radiative) cooling rate in clusters and galaxies is reduced by at least one order of magnitude with respect to the simple expectation (Peterson et al. 2001, 2003; Xu et al. 2002; Peterson & Fabian 2006, and references therein). This is the so-called ‘cooling flow problem’.

Active galactic nuclei (AGN) can easily provide enough energy to the gas to offset the energy lost by radiation and high resolution X-ray images show indeed clear evidence of AGN-gas interaction in many clusters and galaxies (Boehringer et al. 1993; Blanton et al. 2001; Finoguenov & Jones 2001; Jones et al. 2002; MN07 and references therein). The fairly common presence of X-ray cavities, often coincident with lobes of radio emission connected to the core of the central galaxy by a radio jet, indicates that AGN inject energy in the intracluster medium (ICM) in kinetic form (outflows) and as relativistic particles, although the quantitative significance of the latter is difficult to estimate (Dunn et al. 2005; Gitti et al. 2009).

Rafferty et al. (2006, 2008) showed that the AGN power associated to the cavity formation is of the same order as the core X-ray luminosity, for a sample of 33 clusters and groups. Although this energetic balance is only a necessary but non sufficient requirement for a heating scenario to be successful, it strongly suggests that the heating process manifests itself generating bubbles in the ICM. Cavities can be

\* E-mail: massimo.gaspari4@unibo.it

created only by ‘directional’ input of energy, such as jets or collimated outflows, making spherically symmetric form of heating less appealing as major players in solving the cooling flow problem.

In order to prevent significant gas cooling, the feedback process must be activated with a frequency not greatly different from  $1/t_{\text{cool}}$ , where  $t_{\text{cool}}$  is the central cooling time, often of the order of few  $\times 10^8$  yr for clusters (e.g., Sanderson et al. 2006; Mittal et al. 2009) and even lower for elliptical galaxies or groups (e.g.  $t_{\text{cool}} \sim 1.5 \times 10^7$  yr for NGC 4636, see Baldi et al. 2009).

Moreover, the feedback heating must preserve the cool core appearance of the majority of the clusters (Peres et al. 1998; Mittal et al. 2009). In fact, it has been shown that concentrated heating while very efficient in stopping the cooling process, often generates negative temperature gradients, contrary to the observations (Brighenti & Mathews 2002, 2003; Mathews et al. 2006). Another indication that AGN cannot deposit most of its energy in the very central region is the common survival of galactic scale cool cores in cluster ellipticals (Sun et al. 2005, 2007); a spatially concentrated heating would easily erase these fragile low temperature regions (Brighenti & Mathews 2002, 2003).

Motivated by these considerations, we investigate here the long term effect of kinetic feedback on the ICM (see MN07 and Fabian 2009). We assume that AGN outbursts generate collimated, subrelativistic outflows on kpc scale. There is widespread observational evidence for winds originating in galactic nuclei. High redshift radio galaxies host galactic scale, bipolar outflows of ionized gas with velocity  $\sim 1000$  km s $^{-1}$ , likely triggered by the interaction of the radio jet with the ISM (Nesvadba et al. 2008). Neutral gas is also expelled at a rate of tens  $M_{\odot}$  yr $^{-1}$  by active nuclei (Morganti et al. 2005, 2007). Further evidence for fast AGN outflows come from UV and X-ray observations (George et al. 1998; Crenshaw et al. 1999; Kriss 2003; Risaliti et al. 2005; McKernan et al. 2007; Pounds & Reeves 2009; see Crenshaw et al. 2003 for a review). It is reasonable to conclude that most of the AGN exhibit outflows, albeit the physical parameters of the winds are still uncertain. The geometry of the flow is also unclear, both polar winds, perhaps caused by entrainment of the ICM in the relativistic radio jet, or equatorial disc winds (see Proga 2007 and references therein) being possible.

The key question we want to address in this work is the following: *are outflows from the central AGN able to prevent the ICM from cooling and at the same time preserve the cool core appearance?*

In recent years a considerable amount of research has been devoted to the understanding of the effect of jets on the ICM. Most works investigated the transient flow resulting from a bipolar outflow (Reynolds et al. 2001, 2002; Basson & Alexander 2003; Ruszkowski et al. 2004; Omma et al. 2004; Zanni et al. 2005; Brueggen et al. 2007; Sternberg et al. 2007; Sternberg & Soker 2009), but did not fully confronted the question above.

The long term influence of AGN outflows on cluster cooling flows was studied by Brighenti & Mathews (2006, hereafter BM06). They used 2D simulations and a mechanical feedback scheme, self-regulating injection time (but not velocity and power). They calculated the gas cooling rate and the azimuthally averaged density and temperature pro-

files. It was found that some intermittent bipolar outflow models, with velocity in the range  $5 \times 10^3 - 10^4$  km s $^{-1}$ , could shut down gas cooling for many Gyr, while preserving the cool core appearance of the cluster.

Cattaneo & Teyssier (2007) performed 3D calculations of AGN feedback in a poor cluster, about  $\sim 10$  time less massive than the object studied here. They employed a hybrid kinetic-thermal feedback which injects energy at a rate proportional to the Bondi accretion rate to the central black hole. With the adopted ICM initial conditions the central cooling time is quite long (4 Gyr), and the average cooling rate in absence of feedback is  $\sim 30 M_{\odot}$  yr $^{-1}$ . During the most powerful AGN outbursts only a small fraction of energy is ejected in kinetic form, the velocity of the jets being only  $\sim 1.4 \times 10^3$  km s $^{-1}$ . Their models are successful in stopping gas cooling, but the cool core disappear after a few Gyr.

The present paper builds on the preliminary results by BM06 to explore a larger set of feedback schemes and bound the parameter space for successful feedback models. In this work we use multigrid, 3D hydrodynamical simulations for two reasons. First, the nature of cooling flows is intrinsically chaotic and turbulent, therefore it is essential to allow a realistic description of all instabilities, which in turn influence the outflow evolution. Second, we want also to eliminate the spurious cooling of gas along the  $z$  symmetry axis present in 2D axisymmetric calculations (like in BM06).

As stated above, our primary objective here is to investigate if massive, collimated outflows can provide a suitable form of feedback to solve the cooling flow problem. The adopted scheme for the generation of jets and their connection with the accretion on the black hole is simplified and parametrized (as customary in similar studies), and attempt to investigate subjects like growth of the black hole or jet physics is certainly superficial. We will critically test our models, trying to recognize all the positive and problematic aspects of this form of feedback, comparing our results with a great variety of observational constraints.

Finally, we mention that other authors simulated the feedback from buoyant cavities and the associated shock heating, without explicitly including the jets that likely generate these features in real clusters (Brueggen & Kaiser 2002; Brighenti & Mathews 2003; Ruszkowski et al. 2004; Dalla Vecchia et al. 2004; Brueggen et al. 2005; Sijacki et al. 2007; Brueggen & Scannapieco 2009; Mathews & Brighenti 2008a,b; Mathews 2009; the latter three papers considered cavities generated by cosmic rays). This and other different kinds of feedback will be also explored by us in forthcoming papers.

## 2 THE COMPUTATIONAL PROCEDURE

The simulations presented here were calculated with an highly modified version of FLASH 3.2 (Fryxell et al. 2000), a 3D adaptive mesh refinement (AMR) public code, which solves the hydrodynamic euler equations through a split Piecewise-Parabolic Method (PPM) solver, particularly appropriate to describe shock fronts. It uses the Message-Passing Interface (MPI) library to achieve portability and efficient scalability on a variety of different parallel HPC sys-

tems. The simulations were run on 128 processors of IBM P575 Power 6 (SP6) at CINECA supercomputing centre.

We added several source and sink terms to the usual hydro-equations solved by FLASH, in conservative form:

$$\frac{\partial \rho}{\partial t} + \nabla \cdot (\rho \mathbf{v}) = \alpha \rho_* - q \frac{\rho}{t_{\text{cool}}} + S_{1,\text{jet}}, \quad (1)$$

$$\frac{\partial \rho \mathbf{v}}{\partial t} + \nabla \cdot (\rho \mathbf{v} \otimes \mathbf{v}) + \nabla P = \rho \mathbf{g}_{\text{DM}} + S_{2,\text{jet}}, \quad (2)$$

$$\begin{aligned} \frac{\partial \rho \varepsilon}{\partial t} + \nabla \cdot [(\rho \varepsilon + P) \mathbf{v}] = \rho \mathbf{v} \cdot \mathbf{g}_{\text{DM}} + \alpha \rho_* \left( \varepsilon_0 + \frac{\mathbf{v}^2}{2} \right) \\ - n_e n_i \Lambda(T, Z) + S_{3,\text{jet}}, \end{aligned} \quad (3)$$

$$P = (\gamma - 1) \rho \left( \varepsilon - \frac{\mathbf{v}^2}{2} \right) \quad (4)$$

where  $\rho$  is the gas density,  $\mathbf{v}$  the velocity,  $\varepsilon$  the specific total energy (internal and kinetic),  $P$  the pressure,  $\mathbf{g}_{\text{DM}}$  the gravity of dark matter, and  $\gamma = 5/3$  the adiabatic index. The temperature is computed from  $P$  and  $\rho$  using state Eq. (4), with an atomic weight  $\mu \simeq 0.62$ , appropriate for a totally ionized plasma with 25% He in mass.

Outflow source terms  $S_{1,2,3,\text{jet}}$  (dependent on injected density, momentum and mechanical energy, respectively), along with the spatial distribution of the source region, will be explained for every type of feedback in Section 2.2. Note that injection will be done directly into the domain (without a mass inflow,  $S_1 = 0$ ) or through boundary condition at  $z = 0$  ( $S_1 > 0$ ).

Radiative cooling is treated in the code like a source term in Eq. (3): the ICM loses energy at a volume rate  $n_e n_i \Lambda(T, Z)$ , where  $n_e$  and  $n_i$  are the number density of electrons and ions, and  $\Lambda$  is the cooling function for a temperature  $T$  and metallicity  $Z$  (Sutherland & Dopita 1993). In the following we assume  $Z = 0.3 Z_{\odot}$ , a typical metallicity for these systems (Tamura et al. 2004), ignoring central negative gradients.

We also consider SNIa and stellar winds heating in the central elliptical galaxy ( $\rho_*$  is the de Vaucouleurs stellar density profile), although their effect is minor in massive clusters. They are implemented following the parametrization of Brighenti & Mathews (2002), with a rate (dominated by stellar mass loss)  $\alpha = \alpha_* + \alpha_{\text{SN}} \sim 4.7 \times 10^{-20} (t/t_n)^{-1.3} \text{ s}^{-1}$ , where  $t_n = 13.7$  Gyr is the present time, and with a specific injection energy  $\varepsilon_0$  dependent on SNIa and stellar winds temperature.

We also add a mass dropout term (see also Brighenti & Mathews 2002) to avoid a clutter of zones filled with cold gas, which jet events could spread at larger radii and whose physics cannot be described with the simulations presented here. In order to prevent this feature, we have to include a mass sink term  $-q(T)\rho/t_{\text{cool}}$  in Eq. (1) and drop out the cold gas (at constant pressure), without affecting the hotter flow. Here the dimensionless coefficient  $q(T)$  is defined as  $2 \exp(-(T/T_q)^2)$  and dropout becomes significant when  $T \lesssim T_q = 5 \times 10^3$  K. The cooling time is assumed  $t_{\text{cool}} = 5P/2n_e n_i \Lambda$ . Note that the total mass of cooled gas does not depend on the presence of the dropout term or its functional form (Brighenti & Mathews 2000).

We calculate the flow evolution for 7 Gyr (large cluster formed relatively recently), as opposed to most of the works cited in Section 1. As shown in Section 3.1 several feedback

heating schemes are only able to delay excessive gas cooling for 1-2 Gyr before failing, and therefore we stress the need to investigate the long term (several Gyr) behaviour of heated flows.

## 2.1 The cluster model and initial conditions

As in BM06, we adopt the well observed cluster Abell 1795 (Tamura et al. 2001; Ettori et al. 2002) as a template for our models. Being A 1795 a rather typical, relaxed (Buote & Tsai 1996), cool core massive ( $M_{\text{vir}} \sim 10^{15} M_{\odot}$ ) cluster, all the results we present should be relevant for any object in this category. The short central cooling time,  $t_{\text{cool}} \sim 4 \times 10^8$  yr (Ettori et al. 2002) assures that this cluster should host a strong cooling flow in absence of appropriate feedback. However, recent X-ray observations place an upper limit to the radiative cooling rate  $\dot{M}_{\text{cool}} \lesssim 30 M_{\odot} \text{ yr}^{-1}$  (Peterson et al. 2003; Bregman et al. 2006), which is a key constraint for the success of a model.

We start our calculations with the hot gas in spherical hydrostatic equilibrium in the potential well of the dark matter halo:

$$\frac{dP}{dr}(r) = -\rho(r) \frac{d\phi_{\text{DM}}}{dr}(r), \quad (5)$$

where  $r$  is the spherical radius. The dark matter halo follows a NFW distribution (Navarro, Frenk & White 1996), with virial mass  $10^{15} M_{\odot}$ , and thus a potential given by:

$$\phi_{\text{DM}}(r) = -\frac{GM_{\text{vir}}}{r_s f(c_{102})} \frac{\ln(1+r/r_s)}{r/r_s}, \quad (6)$$

where the concentration at overdensity 102 is  $c_{102} = r_{\text{vir}}/r_s \simeq 6.6$  with virial radius  $\simeq 2.6$  Mpc, and  $f(c_{102}) = \ln(1+c_{102}) - c_{102}/(1+c_{102})$ . We have adopted a  $\Lambda$ CDM cosmological universe with  $\Omega_M = 0.27$ ,  $\Omega_{\Lambda} = 0.73$  and  $H_0 = 71 \text{ km s}^{-1} \text{ Mpc}^{-1}$ .

Combining Eq. (6) and an observed  $T(r)$  fit (see third panel of Fig. 1, dotted line) with Eq. (5), we recover the density radial profile  $\rho(r)$ , assuming an ideal gas  $P = k_b \rho T / \mu m_p$  and a gas fraction of 0.15 at virial radius.

In most models we ignore the contribution to the gravitational potential due to the central galaxy. This is important only in the inner few tens kpc and has no significant effect on the cooling rate or the hydrodynamical variable profiles. In one model we have also included the gravity from the central galaxy, modelled as a de Vaucouleurs profile (Mellier & Mathez 1987) with total stellar mass  $M_* \sim 6 \times 10^{11} M_{\odot}$  and effective radius  $r_e \sim 8.5$  kpc, and verified that its influence on the results is inconsequential (see Section 3.1.3).

The computational rectangular box in all of our models extends slightly beyond the cluster virial radius  $r_{\text{vir}}$ . We simulate just half cluster with symmetric boundary condition at  $z = 0$ , while elsewhere we set prolonged initial conditions with only outflow permitted. Despite the AMR capability of FLASH, we decided to use a number of concentric *fixed* grids in cartesian coordinates. This ensures a proper resolution of the waves and cavities generated in the cluster core by the AGN outflows. We use a set of 9 grid levels (with basic blocks of  $8 \times 8 \times 4$  points), with the zone linear size doubling among adjacent levels. The finest, inner grid has a resolution of  $\sim 2.7$  kpc and covers a spherical region of 100

**Table 1.** Parameters and properties of all simulated models.

Model	Feedback	$\epsilon$ efficiency	$W_{\text{jet}}$ jet width (kpc)	$Z_{\text{jet}}$ jet height (kpc)	$v_{\text{jet}}$ jet velocity (km s <sup>-1</sup> )	$\tau_{\text{jet}}$ duration/cycle (Myr)
CF	no AGN heating	-	-	-	-	-
A1	$\Delta M_{\text{cool}}$	$5 \times 10^{-4}$	2.7	6.8	$(2\epsilon\Delta M_{\text{cool}}c^2/M_{\text{act}})^{1/2}$	self-regulated
A2	$\Delta M_{\text{cool}}$	$10^{-3}$	2.7	6.8	$(2\epsilon\Delta M_{\text{cool}}c^2/M_{\text{act}})^{1/2}$	self-regulated
A2L	$\Delta M_{\text{cool}}$	$10^{-3}$	2.7	17	$(2\epsilon\Delta M_{\text{cool}}c^2/M_{\text{act}})^{1/2}$	self-regulated
A3	$\Delta M_{\text{cool}}$	$5 \times 10^{-3}$	2.7	6.8	$(2\epsilon\Delta M_{\text{cool}}c^2/M_{\text{act}})^{1/2}$	self-regulated
A3L	$\Delta M_{\text{cool}}$	$5 \times 10^{-3}$	2.7	17	$(2\epsilon\Delta M_{\text{cool}}c^2/M_{\text{act}})^{1/2}$	self-regulated
A3S	$\dot{M}_{\text{cool}}$	$5 \times 10^{-3}$	2.7	0	$(2\epsilon\Delta M_{\text{cool}}c^2/\rho_{\text{jet}}A\Delta t)^{1/3}$	self-regulated
A4	$\Delta M_{\text{cool}}$	$10^{-2}$	2.7	6.8	$(2\epsilon\Delta M_{\text{cool}}c^2/M_{\text{act}})^{1/2}$	self-regulated
A4L	$\Delta M_{\text{cool}}$	$10^{-2}$	2.7	17	$(2\epsilon\Delta M_{\text{cool}}c^2/M_{\text{act}})^{1/2}$	self-regulated
A5	$\Delta M_{\text{cool}}$	$5 \times 10^{-2}$	2.7	6.8	$(2\epsilon\Delta M_{\text{cool}}c^2/M_{\text{act}})^{1/2}$	self-regulated
B1	intermittent	-	2.7	6.8	$10^4$	20/200
B2	intermittent	-	2.7	6.8	$10^4$	10/100
B3	intermittent	-	2.7	6.8	$10^4$	1/10
C1	continuous	-	2.7	6.8	$2 \times 10^3$	continuous
C2	continuous	-	2.7	6.8	$6 \times 10^3$	continuous
C3	continuous	-	2.7	6.8	$10^4$	continuous
BONDI	$\dot{M}_{\text{B},10\text{kpc}}$	$10^{-1}$	2.7	6.8	$(2\epsilon\dot{M}_{\text{B}}\Delta tc^2/M_{\text{act}})^{1/2}$	self-regulated
BONDI2	$\dot{M}_{\text{B},5\text{kpc}}$	$10^{-1}$	2.7	0	$(2\epsilon\dot{M}_{\text{B}}c^2/\rho_{\text{jet}}A)^{1/3}$	self-regulated

kpc in radius. In general, grids of every level extend radially for about 40 cells. The relatively low resolution is due to the need of covering large spatial scales (kpc up to Mpc) and at the same time integrating the system for several Gyr, using today's available high-performance computing resources.

## 2.2 Outflow generation

We adopt a purely mechanical AGN feedback in form of nonrelativistic, collimated outflows (similar to BM06). In this paper we show results only for models with cylindrical jets, with velocity parallel to the  $z$ -axis. We have calculated few simulations with conical outflows (with half-opening angle up to 70 degrees – see also Sternberg et al. 2007) and we have verified that they have a similar impact on the global properties of the flow. In fact, the pressure of the ICM collimates the outflows within few tens kpc (see BM06).

We consider several types of feedback. In feedback scheme A an outflow is activated only when gas cools to very low temperature within a spherical region  $r < 10$  kpc, and drops out from the flow. Usually most of the gas cools at the very centre of the cluster. We assume that at any timestep a fraction  $\epsilon$  of the rest mass energy of the cooled gas,  $\Delta M_{\text{cool}}c^2$ , is injected as kinetic energy. Here  $\Delta M_{\text{cool}}$  is the gas mass cooled in a given timestep of the finest grid. This energy is given to the hot gas located in a small region at the centre of the grid (the ‘active jet region’), whose size is indicated in Table 1 and containing a gas mass  $M_{\text{act}}$  (there is no new injected mass in Eq. (1)). At every timestep we set the  $z$  component of the velocity within the active region to  $v_j = (2\epsilon\Delta M_{\text{cool}}c^2/M_{\text{act}})^{1/2}$ , since  $E_{\text{k,jet}} \equiv 0.5M_{\text{act}}v_{\text{jet}}^2 = \epsilon\Delta M_{\text{cool}}c^2$ . We will see (Section 3) that the frequency and strength of the feedback events strongly depend on the mechanical efficiency  $\epsilon$ , which has typical values  $10^{-4} - 10^{-2}$ .

We remark again that this scheme to link gas cooling, black hole accretion and outflow generation does not have a strong physical basis: it must be taken as a simplified way to

implement a self-regulated feedback, which triggers heating only when it is needed to halt ICM cooling. In considering massive slow outflows, we are implicitly assuming that the relativistic radio jet entrains some ICM mass ( $M_{\text{act}}$ ). Moreover, other authors (e.g. Giovannini 2004) found that radio jets in cluster central galaxies are highly relativistic on pc scale, but rapidly decrease to subrelativistic velocities within few kpc from the black hole (especially in Fanaroff-Riley I sources), because of the interaction with the dense ISM in the inner region.

In feedback method B the outflows are triggered intermittently, at fixed times (Table 1) and a fixed velocity  $v_{\text{jet}}$  is given to the gas located in the active region (again  $S_1 = 0$  in Eq. (1)). Feedback scheme B is not self-regulated, but the AGN outbursts are forced to occur with a frequency (typically of the order of  $10^7 - 10^8$  yr<sup>-1</sup>) which agrees with the observational estimates (Sanders & Fabian 2007, 2008). The power of any jet event depends only on the mass present in the source region and is independent of the accretion rate.

Next we run a few models where the outflows are continuously generated, that is at every time step we keep the  $z$ -component of the velocity within the jet active region at a given value, listed in Table 1 (scheme C).

We also adopt a scheme, named BONDI, in which the accretion rate is calculated with the Bondi prescription (see also Cattaneo & Teyssier 2007):  $\dot{M}_{\text{Bondi}} = 4\pi(GM_{\text{BH}})^2\rho_0/c_{s0}^3$ , where  $\rho_0$  is the volume-weighted hot gas density calculated within  $r \lesssim 5$  (or 10) kpc, while  $c_{s0}$  is the mass-weighted sound speed in the same region. Needless to say, the Bondi radius,  $r_{\text{B}} \sim 50$  pc, is far smaller than our resolution limit, so we refrain to attach a strict physical meaning to  $\dot{M}_{\text{B}}$ . In this sense the high mechanical efficiencies (0.1) used for Bondi models are due to the fact that the accretion should be a factor 10-100 larger (because of higher inner  $\rho_0$  and lower  $c_{s0}$ ). This feedback is fundamentally different from feedback A because it produces a self-regulated, quasi-continuous, moderate power AGN activity, in contrast

to the few violent AGN outbursts characteristic of the best models adopting scheme A.

Finally, in BOND12 and A3S the outflow is not injected as usual in the active region, but with a mass, momentum and energy flux through the boundary at  $z = 0$  (thus  $S_1 > 0$ ), with a square area  $-1.35 \lesssim x \lesssim 1.35$  kpc,  $-1.35 \lesssim y \lesssim 1.35$  kpc. The velocity of the jet is then calculated as  $v_{\text{jet}} = (2\epsilon\dot{M}_f c^2 / \rho_{\text{jet}} A)^{1/3}$ , where  $\dot{M}_f$  is the accretion rate of the feedback scheme,  $A \sim 7.3$  kpc<sup>2</sup> is the area through which the jet is injected, and  $\rho_{\text{jet}} \sim 2 \times 10^{-26}$  g cm<sup>-3</sup> ( $\sim 10^{-1}$  the initial central gas density). We fix the temperature of the jet to low values ( $10^7$  K) in order to keep injected thermal energy on negligible levels compared to the kinetic flux.

### 3 RESULTS

We describe in this Section the results for various flows, exploring a large set of feedback parameters. In order to understand the long term behaviour of the models we have evolved them for 7 Gyr. The numerical resolution adopted does not allow a deep study of the disturbances generated by the outflows (such as cavities or shocks). On the contrary, we believe these models are appropriate to investigate the global properties of the flows, such as the cooling rate and the azimuthally averaged density and temperature profiles. The suite of simulations described here is used to thoroughly explore the outflows parameter space in order to bound the region of successful models.

#### 3.0.1 Pure cooling flow

As a reference flow we first calculated a pure cooling flow (CF), where no AGN feedback was used, shown in Fig. 1.

As expected, both density and (mass weighted) temperature profiles steepen in the central region, an effect caused by radiative losses and the consequent subsonic gas inflow. In  $\sim 1$  Gyr the calculated profiles disagree with the observations of Abell 1795, although not by a great extent. It is interesting, however, that the logarithmic slope in the core region of the model temperature profiles at late times is very close to 0.4, which Sanderson et al. (2006) found to be typical in the central region of cool core clusters. The similarity between the temperature distribution in our pure cooling flow run and real clusters, where heating is currently preventing gas cooling, put severe constraints on the feedback process: it must not greatly perturb the temperature profile shaped by radiative cooling. This is a demanding requirement (see also Brighenti & Mathews 2002, 2003).

After few Gyr the flow reaches an approximate steady state (see also Ettori & Brighenti 2008 for a quantitative description of the temporal change in the observable profiles). The bolometric X-ray luminosity slowly increases with time, from  $L_x \sim 1.5 \times 10^{45}$  erg s<sup>-1</sup> at  $t = 0$ , up to  $\sim 2.3 \times 10^{45}$  erg s<sup>-1</sup> at  $t = 7$  Gyr. The growth of the gas density in the cluster core is responsible for the increase of  $L_x$ .

It is interesting to investigate the global energetic budget. The internal energy within  $r_{\text{vir}}$  decreases by  $\sim 5 \times 10^{61}$  erg (that is, of about 1%), while the potential energy drops by  $\sim 4 \times 10^{62}$  erg, considering both the hot gas remaining in the grid and the cooled gas at the centre of the cluster. The kinetic energy is  $\sim 2 \times 10^{58}$  erg and is therefore negligible.

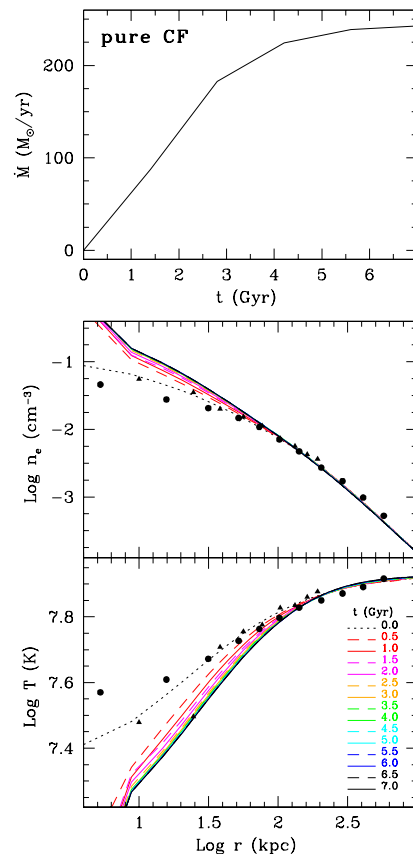


**Figure 1.** Evolution of model CF (no AGN feedback). In the top panel is shown the gas cooling rate versus time. The middle and bottom panels show the temporal evolution of the gas (electron) number density and mass weighted temperature profiles, respectively. The profiles are displayed at 15 different times, as indicated in the lowermost panel. Observational data of A 1795 are shown with filled circles (Tamura et al. 2001, *XMM-Newton*) and filled triangles (Ettori et al. 2002, *Chandra*).

Thus, energy is radiated away ( $E_{\text{rad}} \sim 4.5 \times 10^{62}$  erg in 7 Gyr) mainly at the expense of the potential energy of the ICM.

The gas cooling rate increases with time, reaching  $\sim 250$   $M_{\odot} \text{ yr}^{-1}$  at the end of the calculation, a blatant discrepancy with the observational results (Tamura et al. 2001; Ettori et al. 2002). This is of course the so-called cooling flow problem, the focus of this work. All the gas in this simulation cools in the very centre of the cluster. This findings are in excellent agreement with BM06, showing that these results do not depend on the hydro-code, the coordinate system, the symmetry or the numerical resolution adopted.

In the following we describe the models with jet feedback.

#### 3.1 Feedback A ( $\Delta M_{\text{cool}}$ regulated)

##### 3.1.1 Model A1, $\epsilon = 5 \times 10^{-4}$

We start illustrating results for feedback A models, where the mechanical energy of the jet is linked to the gas mass cooled (within  $r = 10$  kpc). In Fig. 2 we show the relevant properties for model A1, with efficiency  $\epsilon = 5 \times 10^{-4}$ . The

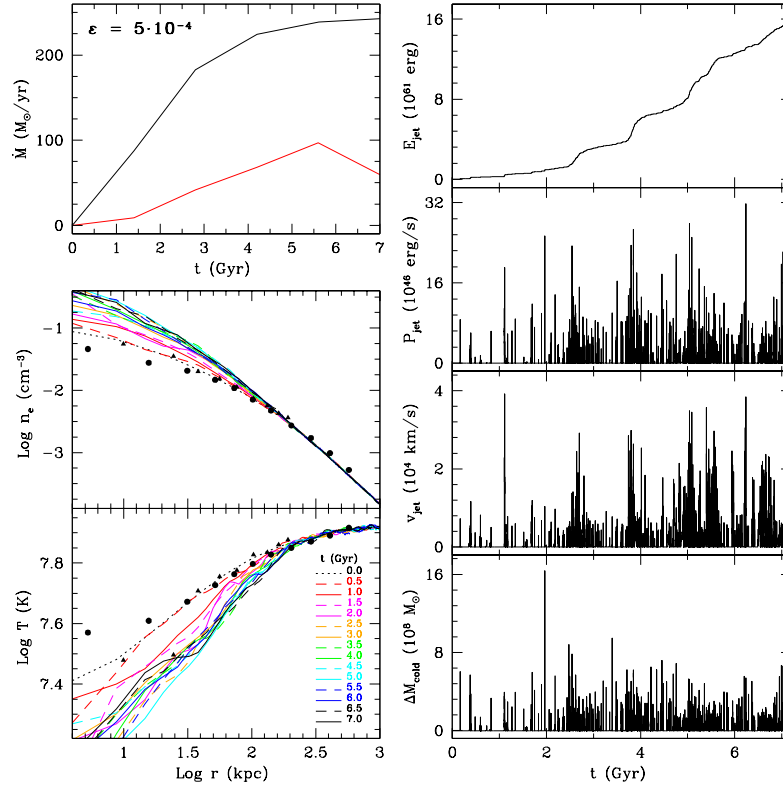


**Figure 2.** Evolution of model A1 ( $\epsilon = 5 \times 10^{-4}$ ). The left column plots are analogous to those in Fig. 1. In the right column are shown the temporal evolution of the total kinetic energy injected by the outflows; the instantaneous power of the outflows; the instantaneous velocity of the outflows; and the mass cooled in a single timestep. These quantities are calculated for the half-space  $z \geq 0$ .

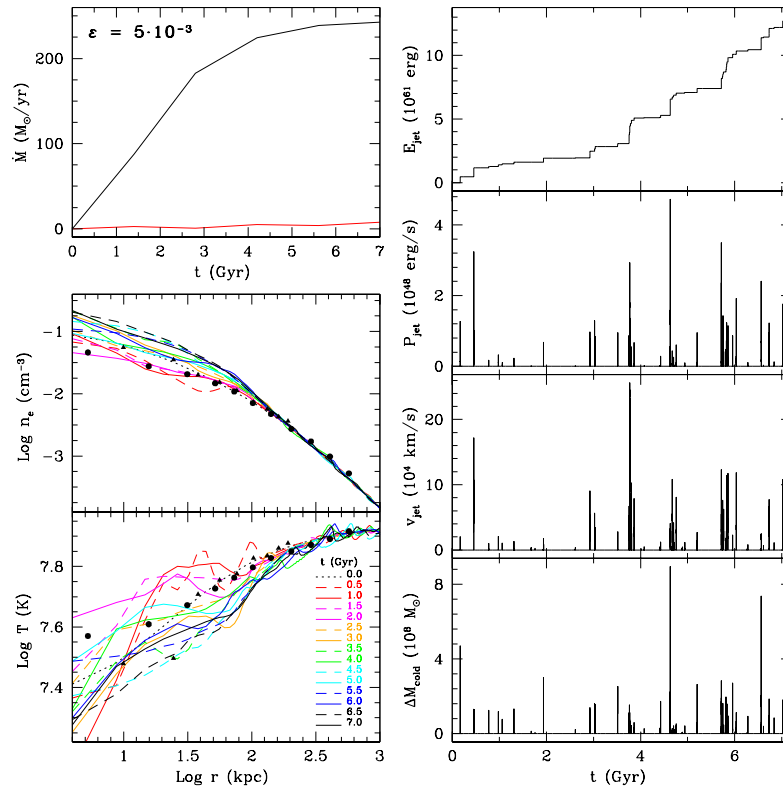


**Figure 3.** Evolution of model A3 ( $\epsilon = 5 \times 10^{-3}$ ). Plots description analogous to Fig. 2.

width and length of the active region are 2.7 and 6.8 kpc (1 and 2.5 grid points), respectively.

The cooling rate, although reduced with respect to the CF model, is still too high ( $\dot{M}_{\text{cool}} \sim 75 M_{\odot} \text{ yr}^{-1}$  at the end of the simulation). The azimuthally averaged, mass weighted temperature and density profiles are similar to those of model CF, with only a little temporal variation: the weak outflows perturb only slightly the temperature profiles.

In the right column of Fig. 2 are shown the physical characteristics of all jet events. In these plots the quantities refer to the half-space  $z \geq 0$  considered in our simulations. In this model the outflows are activated frequently, because their relatively low mechanical power cannot prevent the cooling for a long time.

In the upper panel of the right column is plotted the cumulative (mechanical) energy injected by the jets. At  $t = 7 \text{ Gyr}$ ,  $E_{\text{jet}} \sim 1.5 \times 10^{62} \text{ erg}$  has been injected in the ICM (in the  $z \geq 0$  space). Jets become more frequent at late times, because of the slow secular decrease of the central cooling time, a result of the slight predominance of radiative losses over heating. At the end of the simulation  $\sim 1.6 \times 10^{11} M_{\odot}$  have cooled and dropped out of the hot phase. Clearly, if all the cooled gas were accreted on the central black hole, as we have assumed in our simple feedback scheme, the final black hole mass would result far in excess to that of real black holes. Of course, we could formally avoid the problem of the excessive black hole mass by assuming that only a fraction of the cooled gas actually accretes on it with a higher heating efficiency. For instance, this model would be identical if we assume that only 1% of the cooled gas is accreted by the central black hole and the efficiency is increased to  $5 \times 10^{-2}$ . This degeneracy means that our model is too simple to allow a proper investigation of the black hole growth.

In the remaining panels are displayed the power, velocity and mass cooled (within 10 kpc) during every jet event. Typically, the gas in an outflow is ejected with  $v_{\text{jet}} \approx 10^4 \text{ km s}^{-1}$  and power  $P_{\text{jet}} = 0.5 M_{\text{act}} v_{\text{jet}}^2 / \Delta t \approx 10^{46} - 10^{47} \text{ erg s}^{-1}$ .  $\Delta M_{\text{cold}}$ , shown in the bottom right panel of Fig. 2, is the mass cooled within 10 kpc during a given timestep, has typical values  $10^8 - \text{few } 10^8 M_{\odot}$ . We note that the Eddington luminosity,  $L_{\text{Edd}} \sim 1.5 \times 10^{38} (M_{\text{BH}}/M_{\odot}) \sim 1.5 \times 10^{47} \text{ erg s}^{-1}$  for a  $10^9 M_{\odot}$  black hole, is close to the mechanical power of a typical outflow.

In summary, model A1 ( $\epsilon = 5 \times 10^{-4}$ ) resembles a pure cooling flow model, with a cooling rate still too large and must therefore be rejected. The next logical step is to increase the efficiency  $\epsilon$  in order to reduce the mass of the cooled gas and check if more powerful outflows perturb the variable profiles in an acceptable way.

### 3.1.2 Model A2, $\epsilon = 10^{-3}$

Model A2, with  $\epsilon = 10^{-3}$ , is not shown here and we limit to a brief description of the results. It has good temperature profiles, peaked density profile and a cooling rate of  $\sim 30 M_{\odot} \text{ yr}^{-1}$  at  $t = 7 \text{ Gyr}$ , which is only marginally acceptable. The cooling rate for  $t \lesssim 2 \text{ Gyr}$ , however, is  $< 10 M_{\odot} \text{ yr}^{-1}$ . Evidently, a low efficiency feedback is able to suffocate the cooling flow for several Gyr. Only at late times ( $t \gtrsim 6 \text{ Gyr}$ ) the cooling rate becomes too high. This result emphasizes the importance of calculating a model for many Gyr to check the long term thermal evolution. With respect to

model A1, the jet events are more separated in time, especially at early times, consistently with the low cooling rate at that epoch. The total amount of the energy transferred to the ICM is similar to that for model A1, an indication of the self-regulation of the feedback process.

### 3.1.3 Model A3, $\epsilon = 5 \times 10^{-3}$

The increase of the efficiency to  $\epsilon = 5 \times 10^{-3}$  generates a quite successful model (A3), which we discuss in more length (see also Section 4 for an analysis of the flow dynamics). The cooling rate (Fig. 3) is very low at any time ( $\dot{M}_{\text{cool}} \sim 5 M_{\odot} \text{ yr}^{-1}$ ), a value fully compatible with the current observations ( $\dot{M}_{\text{cool}} \lesssim 30 M_{\odot} \text{ yr}^{-1}$ ; Peterson et al. 2003; Bregman et al. 2006).

The azimuthally averaged density and temperature profiles for  $t \geq 1 - 2 \text{ Gyr}$  are always in good agreement with those observed in A 1795. Both the ICM density and temperature vary somewhat with time, following the outflow cycles as expected, but the cluster always keeps the status of ‘cool core cluster’, even though gas is essentially not cooling. The shock waves generated by the outflows (see Section 4) are not strong enough to significantly heat the gas and perturb the global, azimuthally averaged temperature positive gradient, although small amplitude ripples are seen in the profile, corresponding to weak shocks associated to the jet propagation. These waves are visible up to a distance of  $\sim 400 \text{ kpc}$ .

In this model the AGN feedback is triggered less frequently, and only about 50 jet events occur. The duty cycle is  $\sim 6\%$  (of total time). The total energy injected,  $\sim 1.25 \times 10^{62} \text{ erg}$  is again of the same order as in the previous simulations, and the average power and velocity of the single outflow is therefore larger. This energy must be compared with the total energy radiated away,  $\sim 1.1 \times 10^{62} \text{ erg}$  (again calculated in the half-space  $z \geq 0$ ). Not surprisingly the two energies are of the same order. In fact, if the gas density distribution is similar to that of the standard cooling flow model, then the energy radiated away is also similar. So the energetic balance to stop the cooling requires that AGN provides an energy  $\sim 10^{62} \text{ erg}$ . The power of the outflows often exceeds the Eddington luminosity. While the latter is not strictly relevant in this context, the unpalatable large power might indicate that this feedback fails to simulate the real accretion process at work.

It is instructive to examine the evolution of the energetics in the cluster core region ( $r \leq 50 \text{ kpc}$ ), the most perturbed by the AGN feedback. After every AGN outburst the core kinetic energy increases on average by  $\approx 8 \times 10^{60} \text{ erg}$  (with the most powerful outflows depositing  $\gtrsim 2 \times 10^{61} \text{ erg}$ ), which is comparable to the thermal energy content of the core region ( $E_{\text{th,core}} \sim 1.5 \times 10^{61} \text{ erg}$ ). However, the kinetic energy generated by an outflow is dissipated in only  $\sim \text{few } \times 10^7 \text{ yr}$ . Thus, for most of the time the thermal energy dominates over the kinetic energy. Following the dissipation of the kinetic energy, the thermal energy also rises, because of the shock heating. Finally, a large fraction of the thermal energy gained by the AGN outburst is transformed in potential energy, as a consequence of the quasi-adiabatic cooling due to the expansion of the ICM.

In order to understand the effect of the gravity of the central galaxy, ignored in the models described above, we

have rerun model A3 including its contribution. As expected, being the galactic gravity dominant only in the inner  $\sim 20$  kpc, the basic results (cooling rate and variable profiles) are similar to run A3, and we do not show plots for this model. The only remarkable difference with model A3 is a reduced frequency of the jet, compensated with a larger average power. At the end of the simulation the total energy injected by the outflows in these two models is almost identical.

### 3.1.4 Model A4, $\epsilon = 10^{-2}$

When the efficiency is increased further ( $\epsilon = 10^{-2}$ , model A4, Fig. 4) the overall results are very similar to those for run A3. Again the jet heating generates fluctuations in the temperature which exceed the ones observed now in A 1795. The time averaged profiles (not shown), however, agree very well to the observations. At almost any time this model would be classified as a cool core cluster.

The number of jet activations during the 7 Gyr of evolution is further reduced, with only a few happening within the first several Gyr. The total energy generated by the feedback process is  $\sim 1.5 \times 10^{62}$  erg, again an acceptable value considering that the total ‘available’ BH energy is around  $1.8 \times 10^{62}$  erg ( $E_{\text{BH}} \simeq 0.1 M_{\text{BH}} c^2$ , with  $M_{\text{BH}} \sim 10^9$ ).

### 3.1.5 Model A5, $\epsilon = 5 \times 10^{-2}$

This model (A5,  $\epsilon = 5 \times 10^{-2}$ , Fig. 5) clearly demonstrate the flaws of a too powerful feedback, albeit the total energy generated by the AGN is once more approximately the same as in all the other models. Now the 11 AGN outbursts occurring during the 7 Gyr evolution are quite violent, with power typically larger than  $10^{49}$  erg s $^{-1}$  (right column of Fig. 5). Notice as the outflow velocities approach the relativistic regime. As expected, the gas cooling is essentially zero, but the shock heating is too strong and the central temperature is too high for most of the time. With such an efficient feedback cool core clusters would be a rarity, in contrast to the observational evidence.

### 3.1.6 Model A6, $\epsilon = 10^{-1}$

A feedback with  $\epsilon = 10^{-1}$  (an implausibly large efficiency, but such a model has been calculated for pedagogical reasons; model A6, not shown here) soon erases the initial cool core and the system would show a flat temperature profile thereafter (apart an intermittent mini cool core,  $\sim 10$  kpc in size, associated with the central galaxy and expected also in non cool core clusters; Brighenti & Mathews 2002; Sun et al. 2007; Sun 2009). In passing, we note that the ubiquitous presence of these galactic scale cool cores poses very strict constraints on the nature of the AGN feedback, which can not deposit a large amount of energy in the region near the central black hole.

### 3.1.7 Summary of Feedback A ( $\Delta M_{\text{cool}}$ )

In this section we have illustrated the global features of feedback A models, in order to check whether and when non

relativistic outflows are a tenable mechanism for AGN feedback, able to shut off the gas cooling and at the same time preserving the ‘cooling flow’ appearance ( $T(r)$  and  $n(r)$ ). To summarize the main results, we find that the efficiency must be in the range  $10^{-3} - 10^{-2}$  in order to generate successful models. Outflows must be relatively infrequent and powerful. The total energy necessary to (almost) halt gas cooling for 7 Gyr of evolution is about  $1.5 \times 10^{62}$  erg, not surprisingly of the same order to the energy radiated away. However, the energetic balance *feedback energy*  $\approx$  *energy radiated away* does not guarantee the success of a particular model (see models A1 and A5, for instance). Instead, it is crucial the way this energy is communicated to the ICM, with the appropriate time-scales and power.

## 3.2 Feedback B (intermittent) and C (continuous)

We now illustrate the results when the jets are intermittently activated at predetermined times (feedback scheme B) or by assuming a continuous outflow (feedback C).

In run B1, outflows are generated every 200 Myr by setting  $v_{\text{jet}} = 10^9$  cm s $^{-1}$  inside the active region, for a time of 20 Myr each. The results are shown in Fig. 6, rightmost column. The general features of this model are similar to those of run A2. The cooling rate is very low for the first  $\sim 3$  Gyr and then increases slowly up to  $\sim 80 M_{\odot}$  yr $^{-1}$  at  $t = 7$  Gyr. The variable profiles remind those of a pure cooling flow calculation, especially at late times. This model is acceptable for the first few Gyr. However, the central gas density slowly grows with time until radiative cooling prevails over heating, causing the cooling rate to surpass the threshold of acceptability. The total energy injected by the outflows is  $\gtrsim 2 \times 10^{63}$  erg, a much larger value than in successful simulations adopting feedback scheme A, like A3. This huge amount of energy can not come from a single black hole of typical mass  $\approx 10^9 M_{\odot}$ .

Some of the problems of model B1 can be cured increasing the frequency of the jet events as shown in run B2 (second column from the right in Fig. 6). This model generates outflows every 100 Myr, each one lasting 10 Myr. Their velocity is the same as in run B1. Although the gas cooling rate is much reduced up to  $t = 5$  Gyr, it rapidly increases in the last  $\sim 2$  Gyr. The temperature and density profile gradients become too steep after  $\sim 1 - 2$  Gyr, turning very similar to those of model CF. While these global properties would make this model acceptable, the required total energy is again  $\sim 2 \times 10^{63}$  erg, a value difficult to justify.

A better model can be obtained increasing the frequency of the AGN feedback even further. Model B3, second column from the left in Fig. 6, illustrates a run with outflows activated every  $10^7$  yr (similar to the outbursts frequency estimated for Perseus; Fabian et al. 2006), each one persisting for  $10^6$  yr. As in models B1 and B2, the velocity is set to  $10^4$  km s $^{-1}$ . Only a very small amount of gas cools, and the variable profiles resemble again those of a classical cooling flow. The total feedback energy,  $\sim 1.6 \times 10^{63}$  erg, is still inconveniently large.

The left column of Fig. 6 shows the outcome of a simulation in which the feedback is always active (scheme C). Here the outflow velocity is  $v_{\text{jet}} = 6000$  km s $^{-1}$  (model C2). This is clearly an extreme model that we have calculated mainly for pedagogical reasons. The ICM in the centre is

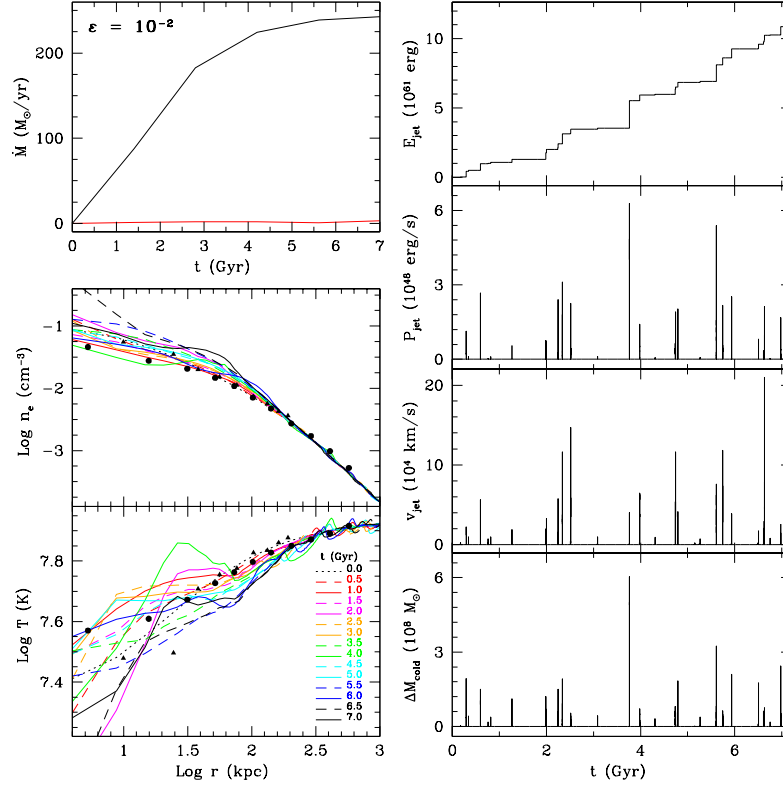


Figure 4. Evolution of model A4 ( $\epsilon = 10^{-2}$ ). Plots description analogous to Fig. 2.

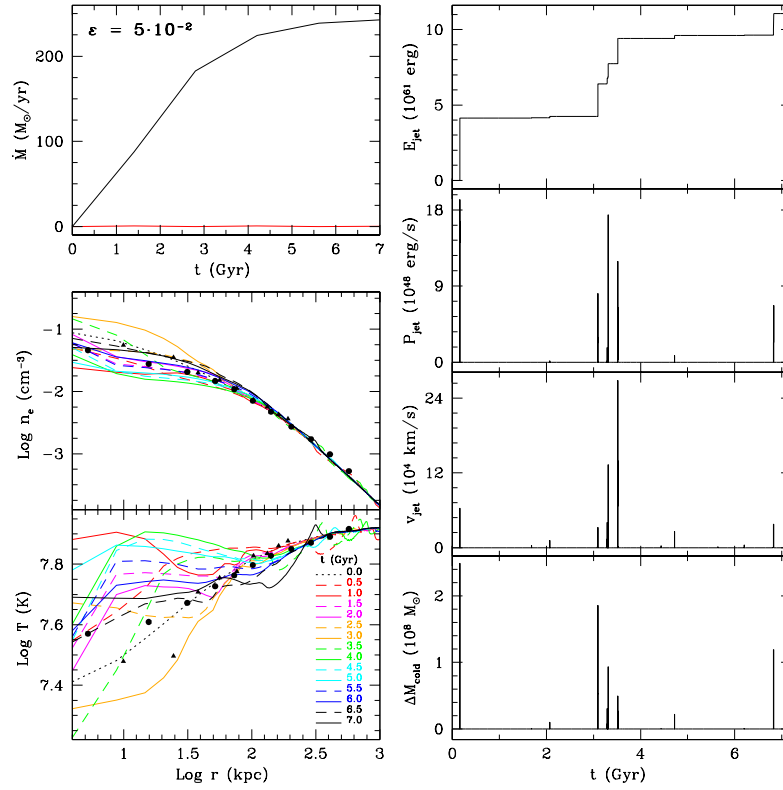
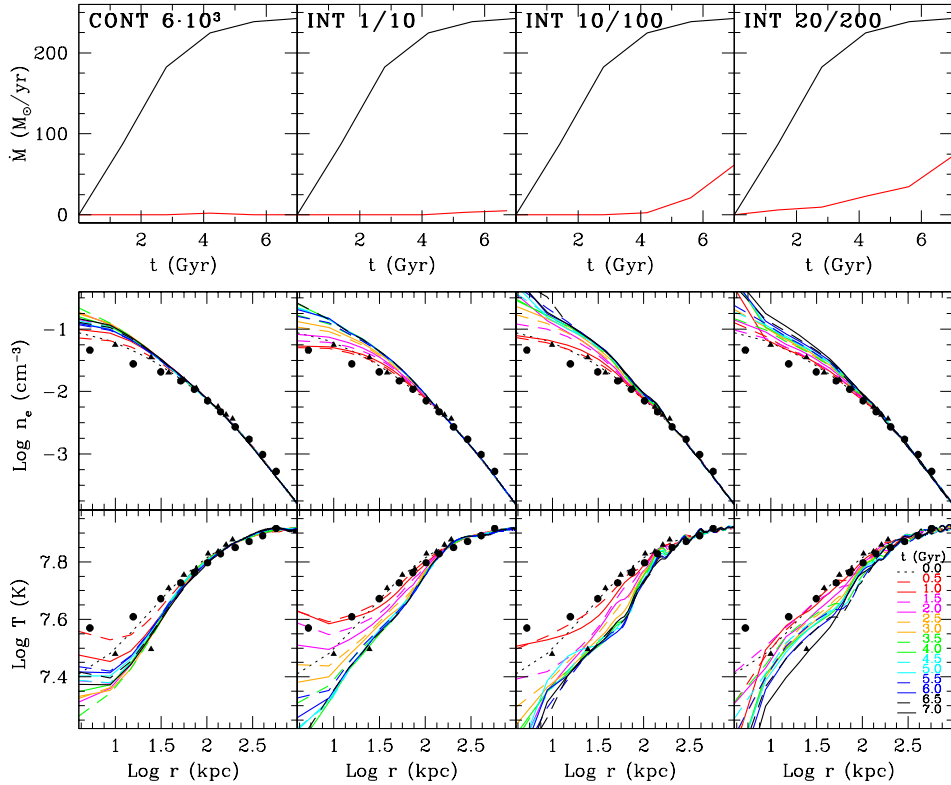


Figure 5. Evolution of model A5 ( $\epsilon = 5 \times 10^{-2}$ ). Plots description analogous to Fig. 2.



**Figure 6.** Evolution of models C2, B3, B2 and B1, from left to right. Plots description analogous to Fig. 1.

continuously heated and transported to large radii, and almost no gas is able to cool. The central density rises secularly and it is possible that some cooling would happen had we evolved the cluster for a longer time. The temperature profiles agree very well with observations, with a flattening due to shock heating visible in the inner  $\sim 10$  kpc. Another unpleasant feature of model C2, besides the excessive injected energy, is that the continuous outflow forms a tunnel in the ICM where it propagates without inflating any cavity (see also the discussion of the Bondi accretion models in Section 3.4).

We have experimented the effect of varying the outflow velocity in feedback C simulations (not shown here). Increasing the jet velocity to  $v_{\text{jet}} = 10^4 \text{ km s}^{-1}$  (model C3) leads to negative temperature gradient in the inner  $\sim 10$  kpc, with  $T(0) \sim 5 \times 10^7 \text{ K}$ , which may be in contrast with the observations of Sun (2009). Conversely, with a reduced jet velocity  $v_{\text{jet}} = 2 \times 10^3 \text{ km s}^{-1}$  (model C1, also not shown here) the gas cooling can not be halted and this cluster resembles a pure cooling flow.

In summary, it is possible to find partially successful models using feedback B or (especially) C, but it is difficult to justify the large amount of outflows energy required or the extreme character of a continuous jet, when we clearly see the signature of intermittent jets and AGN feedback in the different generations of X-ray cavities in many clusters (McNamara & Nulsen 2007; Wise et al. 2007; Fabian et al. 2000).

### 3.3 Role of the jet size

Finally, we address how the results depend on the size of the jet active region. We increased its length to  $\sim 17$  kpc (the width being the same as before, 2.7 kpc) and calculated several models varying the efficiency. We do not show figures for these runs, but only briefly discuss their essential properties. Overall, we find that the results are very similar to those described in the previous section. When the efficiency is  $\epsilon = 10^{-3}$  (A2L model), we find that the cooling rate grows steadily with time, reaching  $\dot{M}_{\text{cool}} \sim 80 M_{\odot} \text{ yr}^{-1}$  at  $t = 7$  Gyr. The temperature and density profiles resemble those for run A2, although they are slightly smoother for  $r \lesssim 20$  kpc, as expected given that the outflow shocks are generated at the tip of the source region, located at  $z \sim 17$  kpc. The run with  $\epsilon = 5 \times 10^{-3}$  (A3L) has excellent attributes, with very low  $\dot{M}_{\text{cool}} \lesssim 10 M_{\odot} \text{ yr}^{-1}$  at any time, and smooth profiles in very good agreement with those observed for A 1795. Finally, we find that high efficiency  $\epsilon = 10^{-2}$  still generates an excellent model (A4L), with very little cooling and very good density and temperature profiles, where a small temperature bump at  $r \sim 30$  kpc, due to the jet shock, is sometime visible in the mass weighted, azimuthally averaged profile.

At the other extreme, we run a model (A3S) in which the jets are generated by imposing a mass, momentum and kinetic energy flux in a small region  $\Delta x = \Delta y = 2.7$  kpc at the centre of the boundary plane  $z = 0$ . Again the outflows are triggered when gas cools, with a given efficiency. The velocity of the inflow is set by the requirement that the kinetic energy injected in a given timestep is  $\epsilon \Delta M_{\text{cool}} c^2$  (see Section 2.2). This scheme, similar to that adopted by

Vernaleo & Reynolds (2006) and Heinz et al. (2006), does not directly change the ICM velocity, but the hot gas is pushed from below by the outflow, which enters the grid at  $z = 0$ . With efficiency  $\epsilon = 5 \times 10^{-3}$ , the same as model A3, we find that the cooling rate (not shown) is acceptable ( $\dot{M}_{\text{cool}} \lesssim 10 M_{\odot} \text{ yr}^{-1}$ ) until  $t \sim 5.5$  Gyr, then increases up to  $\dot{M}_{\text{cool}} \sim 60 M_{\odot} \text{ yr}^{-1}$  at the end of the calculation. The temperature profiles often show a positive central gradient in agreement with the observations of A 1795, although a sharp central temperature peak in the inner  $\sim 10$  kpc is present for  $\approx 20\%$  of the time. We did not pursue the search of the best model using this outflow generation method, by fine tuning the efficiency or other parameters.

We conclude that the size of source region is not a key parameter of our models when the feedback power is linked to the cooling gas, as in the runs presented in Section 3.1.

### 3.4 Feedback triggered by Bondi accretion

As discussed previously, the feedback schemes adopted for the models presented in Section 3 are just a convenient way to link the response of the black hole to the cooling of the ICM, in order to make the feedback process self-regulating. The physics of the accretion, black hole growth and outflow generation, poorly understood in general, is by no means captured in these simulations. This is a general weakness of current models of AGN feedback: the energy (or momentum) is injected in the ICM according to essentially ad hoc prescriptions.

A manifestation of this deficiency is the excessive accretion rates occurring even in our most successful models using feedback A. For instance, in model A4 the most powerful jets ( $P_{\text{jet}} \sim 10^{48} \text{ erg s}^{-1}$ ) imply accretion rates of  $\sim 2000 M_{\odot} \text{ yr}^{-1}$ , much larger than the Eddington rate for a black hole mass of  $3 \times 10^9 M_{\odot}$ ,  $\dot{M}_{\text{Edd}} \sim 60 M_{\odot} \text{ yr}^{-1}$ . These super-Eddington values are not very common for AGN (e.g. King 2009) and yet, according to the results based on feedback A (Section 3.1), we *need* fast and energetic outflows, which imply accretion of large gas masses, to shut down the gas cooling.

At this point we tried a different approach to mitigate this too explosive behaviour. The Bondi accretion theory (Bondi 1952), although highly idealized with respect to the complexity expected in real accretion systems (thin or thick discs, ADAF, etc.), has been widely used to estimate accretion rates on supermassive black holes. However, in presence of a standard cooling flow the ‘unperturbed’ gas is not at rest as in Bondi theory. The accretion rate on the central black hole is then determined by the ICM inflow rate and should be proportional to the cooling rate, which in turn is determined by the global physical conditions of the ISM or ICM. Thus, the Bondi rate should not be particularly relevant if the gas cooling rate is large.

Despite this theoretical consideration, our resolution is still very far from capturing the real central accretion engine (few tens of Schwarzschild radius) and we have to base the triggering mechanism to mean large scale values. In this sense it is interesting to calculate a model in which the AGN feedback is linked to the accretion rate estimated by the Bondi’s formula:  $\dot{M}_{\text{B}} = 4\pi(GM_{\text{BH}})^2 \rho_0 / c_{\text{s}0}^3$  (see Section 2.2). Note that the accretion increases when temperature drops and density grows, or better when the entropy ( $s \propto T/\rho^{2/3}$ )

is falling off. Therefore, also Bondi models are sensitive to gas cooling, but in a more gentle and moderate manner. If such a small accretion rate is sufficient to halt the cooling, then this model is self-consistent.

In a sample of nine X-ray bright elliptical galaxies Allen et al. (2006) estimated typical Bondi accretion rates  $\dot{M}_{\text{B}} \approx 0.01 M_{\odot} \text{ yr}^{-1}$ . For galaxies at the centre of rich clusters the Bondi rates are not expected to greatly exceed these values. Therefore, the Bondi AGN feedback model should operate in an opposite regime than that in models A3 or A4. In particular, we expect a quasi-continuous AGN activity of moderate intensity. Such a model is similar to that calculated by Cattaneo & Teyssier (2007), who were able to drastically reduce the cooling rate (injecting also much thermal energy), although the price to pay for this result was the absence of a cool core.

In the first BOND1 model the outflow is generated in the same way as for feedback scheme A, that is injecting the energy to the gas contained in the active region ( $2.7 \times 2.7 \times 6.8 \text{ kpc}^3$ ), but with an efficiency of 0.1. Note that here we averaged  $\rho_0$  and  $c_{\text{s}0}$  in a radius of 10 kpc from the centre. We do not show figures for this run, but limit ourself to a general description. As anticipated, this model is characterized by an almost continuous activity of relatively weak outflows, with typical velocity of  $\sim 1000 \text{ km s}^{-1}$ . The density and temperature profiles are very similar to those of the classical cooling flow simulation and the cooling rate rises to unacceptable values of  $\sim 250 M_{\odot} \text{ yr}^{-1}$ . This simulation recalls A1: the very frequent, moderate power outflows are not able to prevent massive cooling, resulting in a model almost undistinguishable from a pure cooling flow. It is important to note, that even if the heating is always turned on, the jet power is greatly oscillating from  $10^{43}$  to few  $10^{45} \text{ erg s}^{-1}$ . In fact the Bondi rate feels the low entropy gas which is cyclically building in a small torus, around the perpendicular outflow ( $\sim 10$  kpc). In the end this simulation fails to meet our requisites for a successful model.

In order to make the outflows more steady, in model BOND2 we doubled the grid resolution and halve the averaging zone (now a spherical region of radius 5 kpc). This way the Bondi rate is less susceptible to the cold torus formed in a radius of 10 kpc. To explore Bondi feedback further, we wanted also to use the smallest jet possible, calculating a second model with the alternative jet generation scheme: now the jet (mass, momentum, and mechanical energy flux given by  $0.1\dot{M}_{\text{B}}c^2$ ) is injected from the grid boundary at  $z = 0$  as described in Section 2.2.

The results for this model (BOND2) are shown in Fig. 7. The  $T$  and  $n$  profiles and the cooling rate are good, with the latter exceeding the observational limits only after  $\sim 6$  Gyr. As in the previous Bondi model the activity of the AGN is continuous and moderately weak, but now the jet power is very steady (on the contrary of previous simulation) in the range  $2 - 3 \times 10^{44} \text{ erg s}^{-1}$ , for a total injected energy of  $\sim 7 \times 10^{61} \text{ erg}$ . In fact, the accretion rate does not vary much,  $\dot{M}_{\text{B}} \sim 4 - 8 \times 10^{-2} M_{\odot} \text{ yr}^{-1}$ , slightly larger than the estimates by Allen et al. (2006).

In shrinking the central averaging zone (for the entropy) the Bondi accretion does not present many fluctuations and the triggered outflows seem capable of reducing the cooling flow. This might be more evident with higher resolution (up to Bondi radius) and thinner jets.

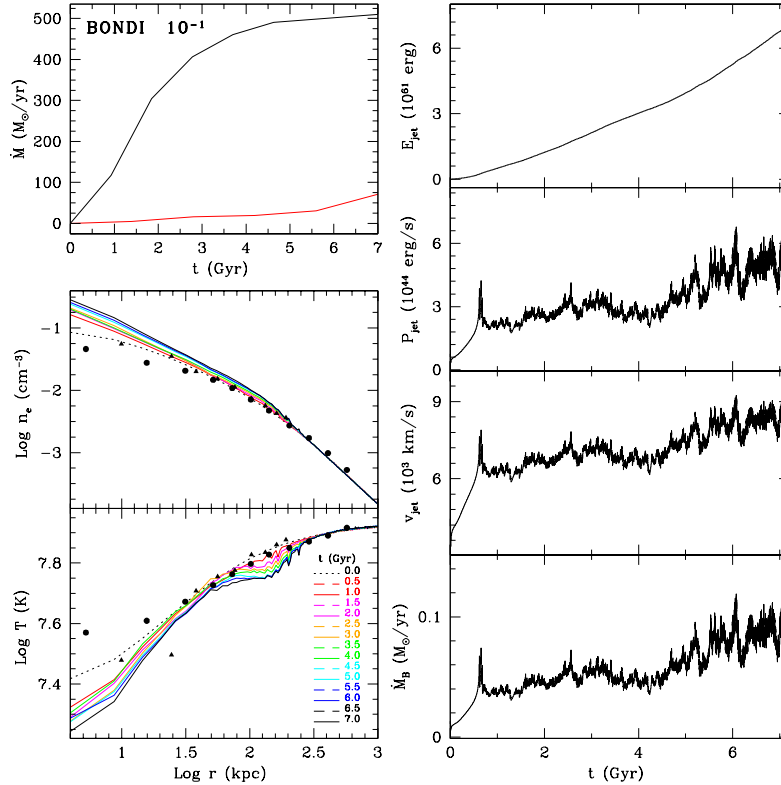


**Figure 7.** Evolution of model BOND12. Here the jet is injected from the grid boundary at  $z = 0$  (see Section 2.2 for details). In the left column are represented the same quantities as in Fig. 2. In the right column are shown, from top to bottom, the total energy injected by the AGN, the instantaneous power of the jet, the velocity of the jet and the Bondi accretion rate, respectively.

Furthermore, comparing both Bondi models, we have noticed that, from a numerical point of view, injection through the boundaries seems a better method to produce a jet and subsequent entrainment (as pointed out by other authors, Omma et al. 2004 for example). This way the jet flux is tightly coupled to the (PPM) hydrodynamical algorithm and not inserted like a split source term, modifying by-hand flow variables in cells of the effective computational domain. Moreover, keeping a fixed jet density, the velocity can not reach very high values (like  $10^5 \text{ km s}^{-1}$ ), facilitating the stability of the code and moderate CFL number ( $\sim 0.4$ ).

A possible riddle for BOND12 model is the absence of frequent jet-inflated spherical cavities (see also model C in Section 3.2). The continuous AGN activity (mean  $v \sim 7000 \text{ km s}^{-1}$ ) carves a narrow tunnel of about 50 kpc in length, although its density contrast with the environment is large only for  $z \lesssim 20 \text{ kpc}$  (and not particularly evident in the SB maps). See Section 6.3 for a deep discussion.

We will certainly extend the study of Bondi-type feedback in a dedicated future paper.

#### 4 DYNAMICS OF MODEL A3

In this Section we will discuss the dynamical evolution of the outflows for one of the best models, A3 ( $\epsilon = 5 \times 10^{-3}$ ). Contrary to the almost steady, and not variegated, evolution of model BOND12, the density and temperature maps (i.e. the  $x - z$  midplane) of A3 show significant temporal variations.

Note that in this Section we are analysing *physical* quantities, while the right comparison with observations should be done through *emission-weighted* ones. We will broaden this aspect in Section 5.

The first outflows is triggered at  $t \sim 160 \text{ Myr}$  (see Fig. 3), with a velocity  $v_{jet} \sim 2 \times 10^4 \text{ km s}^{-1}$ , mechanical power  $P_{jet} \sim 1.3 \times 10^{48} \text{ erg s}^{-1}$  and a total energy injected of  $\sim 4.5 \times 10^{60} \text{ erg}$ . The large jet power is due to our adopted feedback method A, where outflows last only while gas is cooling to low temperatures. This implies that the AGN is active only for few timesteps (typically  $\Delta t \approx 10^5 - 10^6 \text{ yr}$ ), since the jet promptly stops the gas cooling in the central region. During a single timestep large masses of gas can cool (also a result of the coarse resolution used), therefore the energy  $\epsilon \Delta M_{cool} c^2$ , corresponding to the cooled gas mass  $\Delta M_{cool}$ , results in a large, and probably exaggerated, instantaneous outflow power.

In Fig. 8 and 9 are represented density and temperature maps in the  $x - z$  plane (the outflows are generated along the  $z$ -axis) for the first two AGN outbursts. At  $t = 170 \text{ Myr}$  (Fig. 8a), after  $\sim 10 \text{ Myr}$  since the jet started, an ellipsoidal cavity with major (minor) semiaxis of about 15 (10) kpc has been carved, surrounded by a shell of shocked gas, whose density is about twice the ambient density at nearby locations. The temperature of the shocked gas is  $\sim 10^8 \text{ K}$ , about three times that of the unperturbed ICM. Therefore the young cavity, expanding approximately at the sound speed is surrounded by a weak, hot rim. The cavity has a relatively low density contrast with the environment,

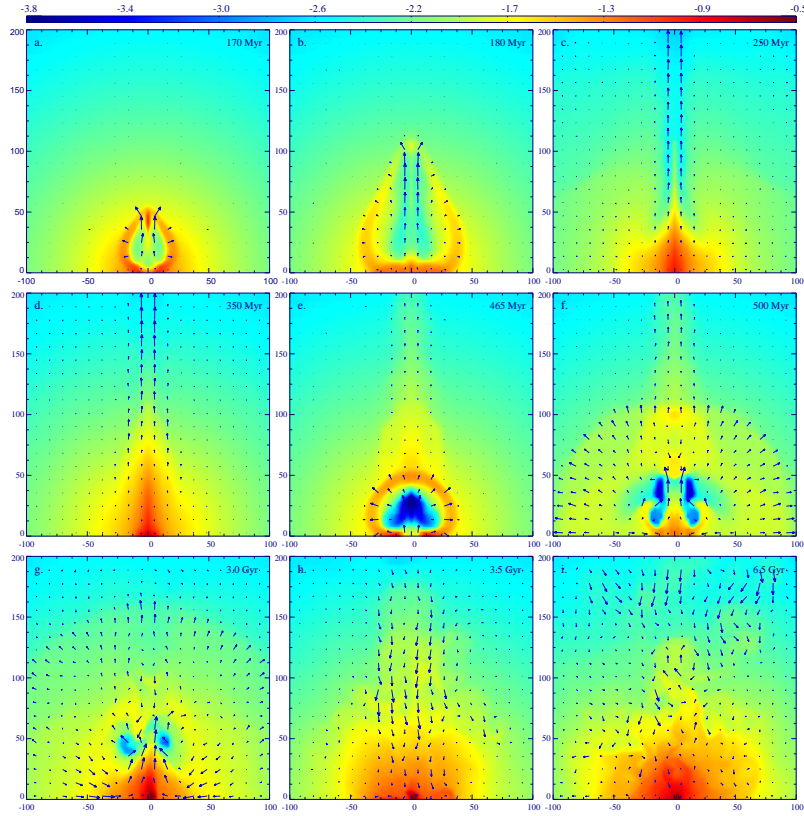


**Figure 8.** A3 model: logarithm maps of electron number density ( $\text{cm}^{-3}$ ) in the  $x-z$  midplane (kpc unit), with velocity field superimposed. The color scale is given by the bar on the top, while arrows length normalization varies. Times are indicated on every top right corner.

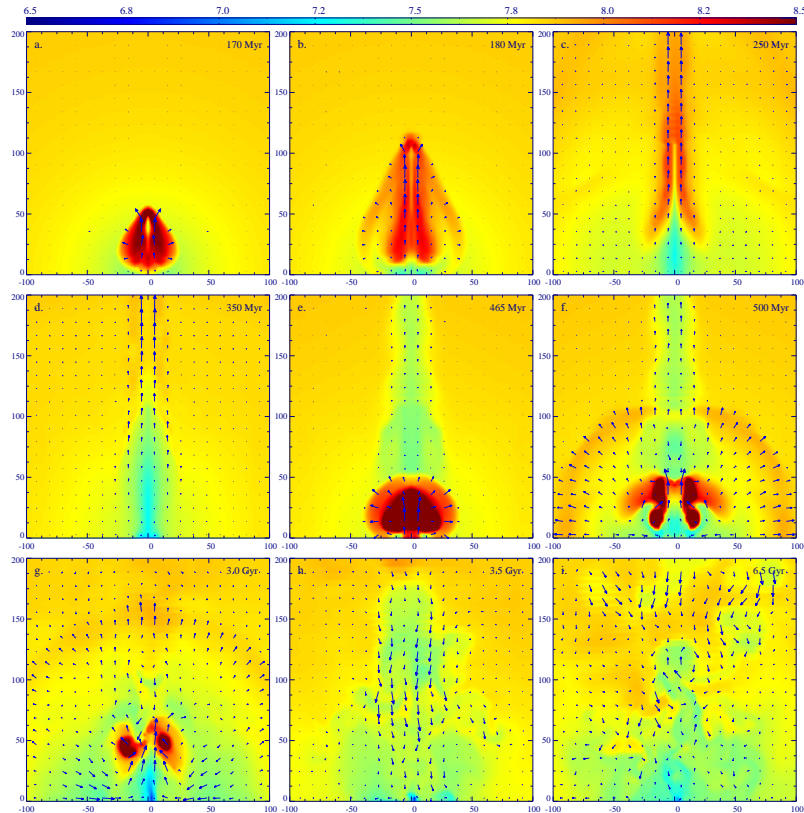


**Figure 9.** A3 model: maps of the logarithm of gas temperature (K). See Fig. 8 for other details.

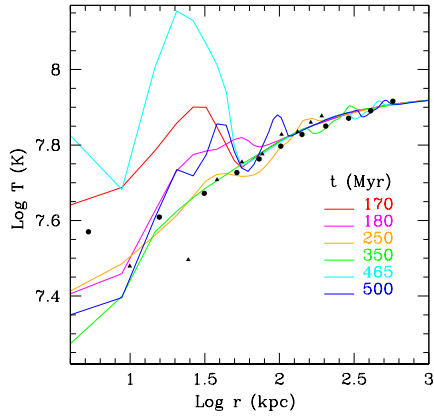


**Figure 10.** A3 model: mass weighted, azimuthally averaged temperature profiles for the six times showed in upper two rows of Fig. 9.

$\sim 3-5$ . Outside the cavity shock the ICM is still slowly flowing in, as a classical cooling flow. The azimuthally averaged (mass weighted) temperature profile (Fig. 10) shows a spike at  $r \sim 30$  kpc, with a fractional increase  $\sim 60\%$ . The cavity expands, increasing its ellipticity, and at  $t \sim 180$  Myr (Fig. 8b) it has approximately a cylindrical shape, extending up to  $z \sim 100$  kpc and with a radius  $\sim 15$  kpc. The bubble is filled with hot ( $\gtrsim 2 \times 10^8$  K) gas raising along the  $z$ -axis at about its sound speed. The density contrast is again 3–4. A very weak ‘pear-shaped’ shock surrounds the cavity. The density gradient along the post-shock region, with denser gas closer to the equatorial  $x-y$  plane, makes the low- $z$  part of the shock detectable, while at large distance from the centre the low density contrast likely prevents the shock detection (see also the X-ray brightness map in Fig. 11). The physical temperature jump across the shock for  $z \lesssim 25$  kpc is only  $\sim 25\%$  and increases slightly at large  $z$ . The structure qualitatively reminds the one observed in the elliptical galaxy NGC 4636 (Finoguenov & Jones 2001; Baldi et al. 2009). In the azimuthally averaged temperature (Fig. 10) the weak shock and the heated gas are visible as a small bump  $\sim 25\%$  in amplitude, located at  $10 < r < 70$  kpc.

20 Myr later the cavity lengthens and narrows, while the back flow generates a dense, relatively cold filament protruding in the cavity (e.g. Mathews & Brighenti 2008a; Gardini 2007). As for the previous times, in most of the volume of the cluster the ICM is inflowing as in a standard cooling flow, and the averaged profiles agree very well with those observed for A 1795; after 40 Myr since the powerful AGN outburst, the cluster fully restored the ‘cool core’ appearance it had at the beginning of the calculation. A very small amplitude ‘ripple’ ( $\Delta T/T \sim 10\%$ ) is visible in the temperature profile at  $\sim 100$  kpc as the integrated effect of the elongated weak shock.

At  $t = 250$  Myr (Fig. 8c) the filament reaches  $z = 100$  kpc, while the cylindrical (subsonic) outflows in the (now almost disappeared) cavity reached  $z \sim 250$  kpc. The temperature ripple moves forward at the sound speed and slowly weakens.

At  $t \sim 350$  Myr (Fig. 8d) the cavity disappears while the dense, relatively cold filament formed by gas formerly at the centre and lifted at large  $z$  by the jet motion, is still

clearly visible. The inner part of the filament, at  $z \lesssim 40$  kpc, reverses its velocity and starts to fall back toward the centre. This is reminiscent of the kinematic of the emission line filaments observed in the Perseus cluster (Hatch et al. 2006). The outer region around the  $z$ -axis is instead still slowly flowing out. This moment marks a new phase in the cluster lifecycle. The fall back of relatively dense gas precludes the next cooling/feedback event, which occurs at  $t \sim 450$  Myr. The feedback cycle starts again in a qualitatively similar way.

Fig. 8e shows the density map at 465 Myr. A new cavity is formed, at first of approximately spherical shape centred at  $z \sim 25$  kpc, radius  $\sim 20$  kpc and high density contrast (50–80). The almost spherical symmetry of the cavity is caused by the inflow along the jet axis, whose ram pressure slows down the expansion along that direction. The shock, already weak (Mach number  $\sim 1.5$ ) is also nearly spherical, with radius  $\sim 35$  kpc.

Again the temperature profile shows the signature of the young AGN outburst with a strong peak for  $r \lesssim 50$  kpc, approximately the location of the shock along the  $z$ -axis. A very weak ripple, vestige of the first jet event, is visible at  $r \sim 400$  kpc.

At  $t = 500$  Myr (Fig. 8f) the cavity shape is strongly affected by the back flow and the density contrast lowers. The weak shock ( $M \sim 1$ ), slightly elongated in shape, is now located at a distance of  $\sim 100$  kpc, much further away than the cavity. Within  $r \sim 100$  kpc the cluster atmosphere is slowly moving outward (with velocity in the range 200–500  $\text{km s}^{-1}$ ). Being the motion very subsonic the density profile changes very slowly. The outflow is decelerating and in  $\approx 100$  Myr reverses its direction approaching the dynamics of a classical cooling flow. Thus, the ICM in the cluster core undergoes cycles of slow contraction and expansion, following the rhythm of the AGN activity.

The cylindrical outflow with average velocity  $v_z \sim 300$   $\text{km s}^{-1}$  along the  $z$ -axis, remnant of the previous AGN outburst is still present, and extends beyond  $z = 200$  kpc. At the same time the inflowing gas in the lower part of the filament is effectively preventing the cavity from expanding or raising buoyantly above  $z \sim 50$  kpc.

Finally, in the bottom row of Fig. 8 we show few snapshots of the density distribution at late times. As the cycle of feedback proceeds the flow develops a more turbulent character. In panel 8g is represented the density map at  $t = 3$  Gyr. The cavity, generated at  $t \sim 2.91$  Gyr, is distorted by the ascending backflow and by falling gas in the filament along the  $z$ -axis. As a result it acquires the shape of an asymmetrical torus. As in the previous aftermaths of the jet episodes, the ICM is flowing inward in most of the cluster volume, and is deviated outward along the  $z$ -direction when it reaches  $r \sim 20$  kpc.

Panel 8h illustrates the cluster during a quiescent period ( $t = 3.5$  Gyr), just before a jet is triggered. The density distribution is very smooth and the cluster appearance is that of a standard cooling flow (see also the profiles in Fig. 3). A large, slightly overdense region around the  $z$ -axis is falling toward the centre with velocity varying between 50 and 500  $\text{km s}^{-1}$ .

Finally, in panel 8i we show the density distribution at  $t = 6.5$  Gyr, again in an epoch long after an AGN outburst. Again, the density is smooth in the core region, while shows

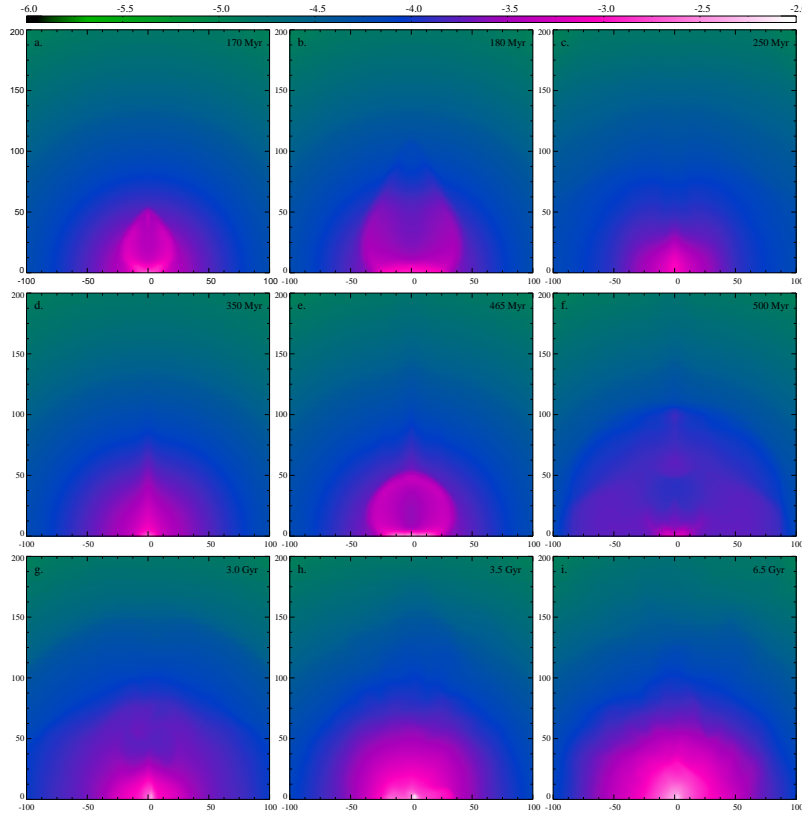


Figure 11. X-ray surface brightness maps for model A3 at various times. The  $x$ -axis is horizontal, while the  $z$ -axis is vertical (kpc units).

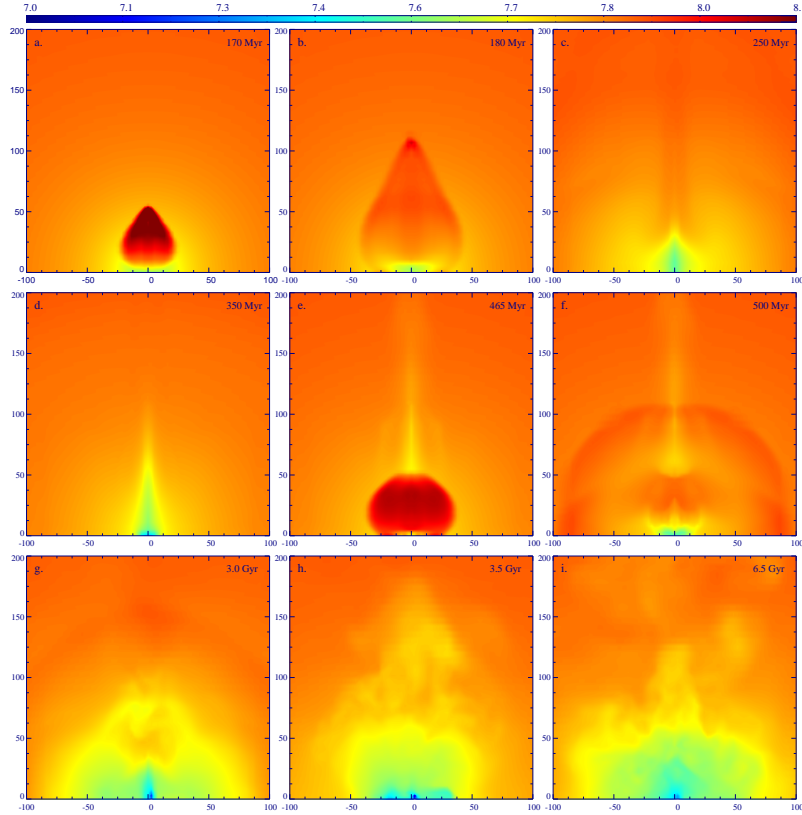


Figure 12. Emission weighted temperature maps for model A3 at various times (see also Fig. 11).

some variation for  $r \gtrsim 50$  kpc. On the contrary, the velocity field is chaotic and very subsonic; it promotes mixing of the metals produced by the SNIa exploding in the central galaxy (see Section 5.3). Few streams of moderately overdense gas are falling from large radii  $r \gtrsim 100$  kpc with velocity  $\sim 300$  km s $^{-1}$ .

## 5 X-RAY OBSERVABLE PREDICTIONS

The  $x-z$  cuts through the centre of the cluster are very useful tools to investigate the intrinsic dynamical evolution of flow variables, like density, temperature and velocity. However, in astrophysics we are limited to observations based on the surface brightness (SB) in a typical spectral range (in our case X-ray band). In theory we have to mock every aspect of the observation, from different atomic emissions to instrument response. Due to our limited resolution, it is sufficient for us to just integrate the emissivity or emission-weighted quantity along line of sight ( $y$ -direction) in an energy range of the X-ray band  $\sim 0.5 - 10$  keV (similar to *Chandra*). In order to obtain more precise SB maps, we developed a parallel code that is able to interpolate every slice of the data cube in 3D (because of the AMR oct-tree) and then perform the above mentioned integration.

With these maps we can test further the observability of our models and, in the lack of real ones, just make predictions that could be in the near future verified or falsified. We will also test common assumptions regarding gas hydrostatic equilibrium, taken in many observational analysis, that seem too restrictive.

### 5.1 Cavities and shocks

We begin investigating the detectability of faint features, like X-ray cavities and shock waves, generated by the AGN outflows. In Fig. 11 we show the X-ray surface brightness maps for run A3, at the same times showed in Fig. 8 and 9. The emission weighted temperature map is displayed in Fig. 12. X-ray depressions are clearly seen at  $t = 180, 465, 500$  and 3000 Myr. Evidently, subrelativistic, massive, collimated outflows can generate cavities with typical diameters of 15-40 kpc. Often the X-ray bubbles are surrounded by bright rims of shocked gas. Relatively weak waves are present at large distance from old cavities, both features being generated by the same AGN outburst.

To better quantify the brightness perturbations produced by the outflows we show in Fig. 13 the profiles along the  $x$ -direction at  $t = 465, 500$  and 3000 Myr, taken at  $z = 25, 50, 50$  kpc, respectively. The sharp jumps at  $x \sim \pm 30$  kpc at  $t = 465$  Myr, where the cavity shock increases the brightness by a factor  $\sim 2.5$  would be manifestly visible in the X-ray image. The relative central depression (the cavity) is indeed brighter than the same region before the jet activity. The emission weighted temperature map reveals that the cavity region is markedly hotter (by  $\sim 80\%$ ) than the nearby ICM, which is not commonly observed. This is a consequence of the infrequent, but explosive outflows like those of model A3.

The maps and profiles at  $t = 500$  Myr show a weak cavity centred in  $y \sim 30$  kpc, with radius  $\sim 20$  kpc. This cavity is also slightly hotter than the surrounding gas. At this time

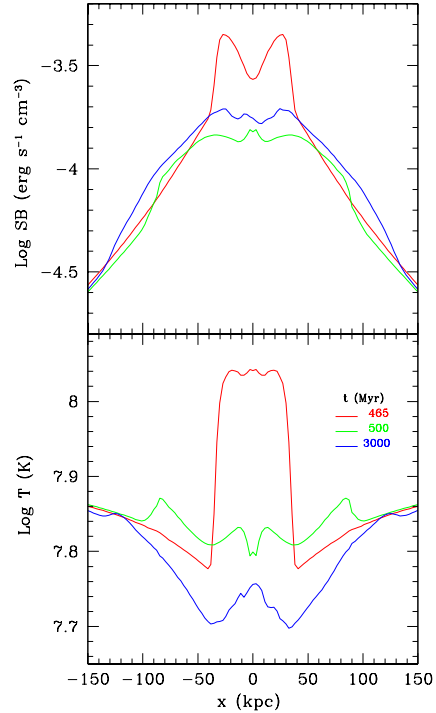


**Figure 13.** A3 model: X-ray surface brightness and emission weighted temperature 1D cuts (of Fig. 11 and 12 maps), through  $z = 25, 50, 50$  kpc, at 465, 500, 3000 Myr, respectively.

the most interesting feature is the weak shock located at a radius  $\sim 100$  kpc: Mach number is  $\sim 1.1$ , in good agreement with observations of shocks driven by AGN (Blanton et al. 2009). The surface brightness profile shows a clear front at the shock position and the emission weighted temperature jumps of  $\sim 10\%$ .

At  $t = 3$  Gyr another weak cavity, again  $\sim 20$  kpc in radius, is present. The brightness depression is only  $\sim 10\%$  and the temperature is higher than the ambient one by the same percentage.

To summarize, our best models presented in Section 3.1, with relatively powerful and infrequent outflows, have the tendency to produce cavities in a violent way, generating shocks which heat much the surrounding ICM. This is also a reason why we investigated the effect of a weaker and quasi-continuous self-regulated feedback (Section 3.4). We will discuss the differences in Section 6.

### 5.2 Iron enrichment and mixing

It is expected that directional outflows would generate metal inhomogeneities through the ICM. Iron is the most relevant and easily measured element, being produced mostly by SNIa, which are still exploding in the giant elliptical at the centre of cool core clusters. The same outflows, however, generate turbulence and bulk motion, which in turn tend to stir and mix the ICM, restoring homogeneity and erasing abundance gradients.

We present here a brief analysis of the emission-weighted iron abundance evolution for model A3. We model only the Fe-enrichment produced by the SNIa (and stellar winds) occurring in the central galaxy, in the time interval

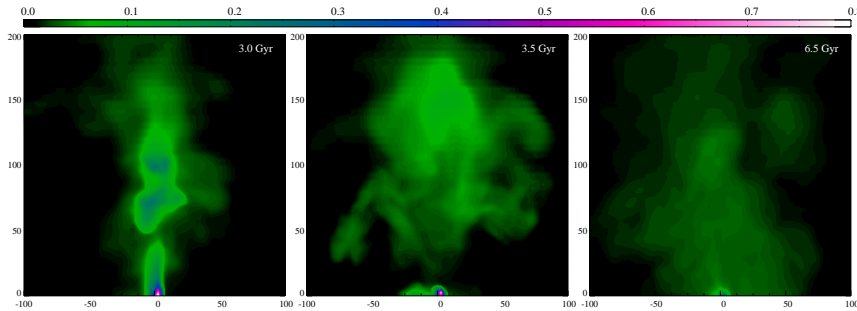


**Figure 14.** Emission-weighted iron abundance maps ( $Z_{\odot}$  unit) in the  $x - z$  midplane for model A3, at three different late times.

6.7 – 13.7 Gyr, the latter being the current age of the universe  $t_n$ . Neglecting the iron produced by the SNI and by the other cluster galaxies, we are not in the position to investigate the complete chemical evolution of the cluster (this will be the subject of a future work). Instead, we are interested here in quantifying the abundance anisotropies caused by the AGN outbursts.

The current SNIa rate is assumed to be  $\sim 0.1$  SNU (supernovae in 100 yr per  $10^{10} L_{B,\odot}$ ), slightly below to that estimated in local early-type galaxies (Cappellaro et al. 1999) but in agreement with the value necessary to generate the observed abundance in well observed giant elliptical galaxies (Humphrey & Buote 2006; Mathews & Brighenti 2003). The time dependence of the SNIa rate is assumed to be  $\propto (t/t_n)^{-1.1}$  (Greggio 2005).

The iron density is implemented in the code as a tracer of the flow ( $\rho_{\text{Fe}} = \phi_{\text{Fe}}\rho$  with  $\phi_{\text{Fe}}$  a scalar between 0 and 1), following the usual advection equation:

$$\frac{\partial \rho_{\text{Fe}}}{\partial t} + \nabla \cdot (\rho_{\text{Fe}} \mathbf{v}) = S_{\text{Fe}},$$

where the source term  $S_{\text{Fe}}$  depends mainly on  $\alpha_{\text{SNI}^*}$  (Sec. 2), as previously discussed (see Mathews & Brighenti 2003 for more details).

In Fig. 14 we present the  $Z_{\text{Fe}}$  maps for model A3, at three different late times. Note that the background (black) is zero, but in reality should be around  $0.3 Z_{\odot}$ : here we are just interested in the contrast. At 3 Gyr (first panel) the abundance is highly asymmetric. A powerful jet event has recently occurred (see Fig. 3), therefore the metals created in the central elliptical galaxy (within few kpc) are transported out along the  $z$ -direction up to a distance of 150 – 200 kpc. This is an unmistakable mark of the presence of a powerful AGN outflow. In fact we suggest that iron abundance can be used as a reliable tracer for any AGN jet-outflow activity, instead of common entropy maps. At the centre the abundance is about  $0.4\text{--}0.6 Z_{\odot}$ , while further away along jet axis the contrast is  $0.1\text{--}0.2$ . This kind of feature is supported by recent deep *Chandra* observations done by Kirkpatrick et al. (2009). They produced Fe-maps showing the enrichment of gas along the jets of Hydra A, a quite massive galaxy cluster. It is striking that our simulated maps resemble these observations also in a quantitative way. Other authors, Doria et al. (in preparation), found a similar behaviour in a different cluster dominated by AGN activity (RBS797).

At 3.5 Gyr (second panel) we are in a period of relatively quiescence and so the now dominating (AGN induced) turbulence and vorticity promote the iron diffusion. At the

centre, the new iron cloud associated to the cD galaxy is clearly detached from the older ejected material, the latter covering now a more uniform area. The iron diffusion is more evident at 6.5 Gyr (third panel), again in a moment of AGN quiet, where the iron is very diffuse, with a low enhancement of  $0.05\text{--}0.1 Z_{\odot}$ .

In the end we can affirm that in a single cycle the iron abundance passes from a phase of high asymmetry along jet axis, when the outflow has recently turned on, to a phase of turbulence and mixing, in which spherical symmetry is almost restored. The iron gets spread within few 100 kpc, just as observed: without the influence of an AGN such material would be indeed confined near the effective radius of the central galaxy.

### 5.3 Hydrostatic equilibrium

In this Section we investigate the effect of the perturbations generated by the AGN outflows on the mass determination using X-ray observations (through Eq. (5)). A standard method to estimate galaxy cluster mass profiles is to assume spherical symmetry and estimate the gravitational mass using the hydrostatic equilibrium equation (e.g. Buote et al. 2007; Vikhlinin et al. 2006 for two recent compilations). When the flow velocity is much lower than the sound speed, the hydrostatic assumption is fully justified.

It is well known that in real clusters turbulence or large scale motion can systematically bias the mass estimate by  $\lesssim 20\%$  (Nagai et al. 2007; Rasia et al. 2006). Therefore, it is interesting to investigate how much the flow perturbations generated by the AGN feedback affect the mass measure.

Here we quantify the discrepancy between the estimated gravitational mass and the real one for a model adopting feedback scheme A and one assuming the more quiet feedback Bondi. We have calculated the azimuthally averaged density and emission weighted temperature profiles in rings of progressively increasing width, from 10 kpc in the centre up to 100 kpc at large radii. These profiles, inserted in the hydrostatic equilibrium equation give the estimated mass profile. This procedure is not perfectly accurate: we should have ‘observed’ our simulations with specific softwares like X-MAS (Gardini et al. 2004; Rasia et al. 2008) or XIM (Heinz & Brueggen 2009) to properly compute the averaged profiles. However, it is not the purpose of this paper to thoroughly investigate this topic and our approximate analysis is sufficient to make our point.

The calculated mass profiles at various times, as well as

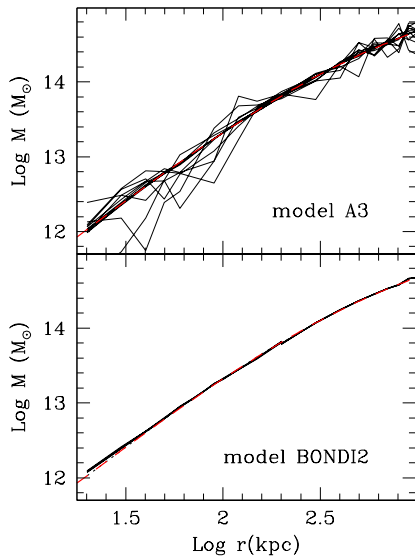


**Figure 15.** Mass profiles for model A3 (top panel) and BONDI2 (bottom panel), calculated using the hydrostatic equilibrium equation at times separated by 0.5 Gyr (model A3) and by 1 Gyr (model BONDI2), and the exact mass profile (red dashed line).

the exact mass profile, are shown in Fig. 15 for model A3 (top panel) and BONDI2 (bottom panel).

In run A3 the powerful outflows, although not able to significantly perturb the thermal state of the cluster (which always preserves the cool core appearance), are effective in disturbing the quasi-hydrostatic equilibrium present in the pure cooling flow model. This results in a typical error in the mass determination of a factor 2-3. Most likely the estimated mass is lower than the real one, and the discrepancy is larger in the region  $r \lesssim 100$  kpc, where the feedback affect the ICM the most.

In model BONDI2, instead, the outflows are 3-4 orders of magnitude less powerful and, despite the fact that they are continuously generated, they seem rather innocuous for the dynamical state of the ICM and the hydrostatic equilibrium approximation is safe. The computed mass profile agrees very well with the real one, with slight discrepancy only visible for  $r \lesssim 20$  kpc, a region inadequately resolved in our simulations. Of course, the weak, continuous jets present in this run are incapable to generate cavities (see Section 3.5), hence it is likely that real clusters undergo at least few stronger AGN outbursts, after which the dynamics of the ICM would be similar to that described for model A3.

In summary, we expect that for clusters where X-ray cavities and/or shocks are present the total mass estimated through the assumption of hydrostatic equilibrium might be in error by a factor of  $\sim 1.5$ , occasionally the error could get as large as a factor of 2-3. Conversely, with gentler continuous outflows generated by the relatively accretion rate predicted by Bondi theory, the estimated and the real mass are in excellent agreement, with errors always below 8% (see also Guo & Mathews 2010).

## 6 DISCUSSION

In this paper we have presented several moderate resolution simulations of the interaction between AGN outflows and the ICM in massive galaxy clusters. The purpose of these calculations was to investigate if a purely mechanical AGN feedback of this kind is able to solve the so called *cooling flow problem*: the dearth of cooling gas in cool core clusters with short central cooling times.

The necessity of covering a large range of spatial (kpc up to 5 Mpc) and temporal scales (fraction of Myr up to 7 Gyr) limited our resolution of the very inner accretion region. Hence we had to link the feedback to some large scale mean quantity, like  $\Delta M_{\text{cold}}$  or  $\dot{M}_{\text{Bondi}}$ , with the obvious result of some discrepancies with observables (like bubbles). In any case gas accretion onto the SMBH and subsequent jet-outflow ignition is still obscure, in particular the amount of ICM entrained and shocked. Furthermore, we do not have a long term (Gyr) evolution of theoretical models for accretion, due to computational limitations. In the end our simplified scheme seems a good and efficient method to test AGN feedback on galaxy cluster scales.

### 6.1 Comparison with other works

In the field of simulated AGN feedback most of the work done in the past (Brueggen & Kaiser 2002; Brighenti & Mathews 2003; Ruszkowski et al. 2004; Dalla Vecchia et al. 2004; Brueggen et al. 2005; Sijacki et al. 2007; Brueggen & Scannapieco 2009; Mathews & Brighenti 2008a,b; Mathews 2009) has focused on the creation of ‘artificial’ bubbles off-centre. This scenario is motivated by the fact that relativistic radio jets (distinct from our outflows) do not entrain much gas and just thermalize the ICM at the hotspot, generating a cavity.

The difference with our study is that we employ a momentum-driven heating, instead of a pressure-driven one. As we have seen, purely kinetic feedback changes the whole dynamics. Intermittent bubbles are naturally created, but this shocked and expanding gas is just one element of the heating process: the bow shock, the cocoon with entrained gas, the mixing through turbulence and vorticity are all fundamental gears of the machine, everyone dominant at different phases of evolution. Moreover, artificial (hydrodynamical) bubbles becomes unstable rapidly; on the contrary some studies (Sternberg et al. 2007) indicate that jet-inflated ones may stay intact for over 40 Myr, thanks to the vortex formed inside. It is probable that a combination of the two mechanisms is required (outflow plus artificial buoyant bubble), even if it still unclear which of the two dominates.

It is difficult to compare our work with other kinetic outflows simulations (e.g. Ruszkowski et al. 2004; Omma et al. 2004; Zanni et al. 2005; Sternberg et al. 2007), because most of them do not implement radiative cooling and an initial cool core state. Additionally, they last for few hundreds Myr and are not suited to study the ‘cooling flow problem’, without the long term evolution.

The only investigations done in this direction are those of BM06 and Cattaneo & Teyssier 2007. In the first one, as many previous studies, the jet velocity and power were set by-hand following observational estimates. We have seen (feedback scheme B), that in imposing such predetermined

conditions, the mechanical feedback is not linked to the cooled mass or lower gas entropy (in quantity and time). The results are models with temperature and density profiles similar to a pure cooling flow or with high cooling rates.

In Cattaneo & Teyssier (2007) the injection scheme is self-regulated by Bondi accretion (for 12 Gyr), but after a weak burst of  $\sim 10^{45}$  erg  $s^{-1}$  the profiles do not present the cool core appearance (flat temperature). Also our successful Bondi model is able to prevent the cooling catastrophe. The difference is that our profiles present ripples and signature of weak shocks. It is again difficult to make a full comparison, because a large fraction of their injected energy is thermal, not only kinetic. In any case, we underline the fact that both results give one clear indication: AGN outflows are a fundamental component of the feedback in galaxy clusters.

The last comparison is the one with Vernaleo & Reynolds (2006). They implemented a self-regulated mechanism similar to our boundary injection scheme. Their simulations present very different results from our (and Cattaneo et al.) analysis. After few hundreds Myr (with every AGN model) the cooling becomes catastrophic:  $> 2000 M_{\odot} \text{ yr}^{-1}$ . The problem of the creation of an unidirectional channel and subsequent deposition of energy is a difficulty found also in our outflow models, but partially resolved in the long term (see Section 6.3.1).

In the next Sections we will deeply discuss the merits and flaws, previously introduced, of our simulated feedback models.

## 6.2 Cold-regulated explosive feedback (A)

In all our study we covered a wide ‘zoology’ of triggering mechanisms, varying the mechanical efficiency and injection method.

In the first series of models we linked the power of the AGN outflows to the cooling rate (feedback scheme A, Sections 3.1), the latter being calculated as  $\Delta M_{\text{cool}}/\Delta t$ , where  $\Delta M_{\text{cool}}$  is the mass of gas cooled within the region  $r \lesssim 10$  kpc in a single timestep  $\Delta t$ . It is clear that the energy of a single jet event depends on numerical resolution through the Courant-Friedrichs-Lewy (CFL) stability condition. Lower resolution calculations, with larger  $\Delta t$  and thus larger  $\Delta M_{\text{cool}}$ , will generate more powerful outburst events.

Although in the models described in Section 3.1 the total kinetic energy injected at a given time rests on the integrated cooled gas mass (which is only weakly dependent on the numerical resolution), and can in principle vary among different models (i.e. different  $\epsilon$ ), we find, somewhat surprisingly, that it is insensitive on the efficiency  $\epsilon$  and always about  $2 - 3 \times 10^{62}$  erg, a value comparable to the total energy radiated away. Evidently, the self-regulation mechanism assumed is very effective.

The first astrophysically important result of these calculations is that the effect of the feedback crucially depends on the modality of the energy injection, not only on the total amount of energy. We have found that when the efficiency is low and the outflows are frequent and relatively weak (models A1 and A2), the gas cooling proceeds at a rate much higher than the limit allowed by observations.

Conversely, when  $\epsilon \gtrsim 0.01$  (models A5 and A6) the cooling rate is reduced to a value fully consistent with the observational constraints. However the ICM in the core is

heated too much and the temperature and density profiles do not resemble those of a typical cool core cluster.

Only models A with efficiency in the range  $5 \times 10^{-3} \lesssim \epsilon \lesssim 0.01$  are able to reduce the cooling rate to acceptable values preserving at the same time a central positive temperature gradient. Moreover, these models generate cavities and shocks, another important requirement that a plausible heating scenario must satisfy. Notice that also observational data (Merloni & Heinz 2008; La Franca et al. 2010) suggest an average mechanical efficiency of AGN around  $5 \times 10^{-3}$ .

As pointed out before, other more ad hoc types of feedback (not directly linked to cooled gas), like intermittent (B) or continuous with fixed velocity (C), present a cooling flow appearance, in the former case, or a too high total energy injection, in the latter. These models are not totally disastrous and show some good features (as found in BM06), but in the long term they are not satisfactory.

### 6.2.1 Riddles

Adopting a severe critical point of view, successful A models may present two difficulties. First, gas often cools and accretes onto the black hole at a rate far above the Eddington limit (section 3.4), a fact which make them unpalatable (King 2009), but not impossible (especially at higher redshift, see for example Szuszkiewicz 2004; Ghosh et al. 2010). It is known that BHs grow mainly through the ‘QSO phase’, that is through radiative accretion at early times (Hopkins et al. 2006). Therefore our accretion rates seem overestimated, considering that the BH mass should not increase much in the entire simulation time.

Remember, however, that our resolution does not permit to track the exact amount of accreted material on sub-pc scale. Hence it is probable that only a small part of  $\Delta M_{\text{cool}}$  falls onto black hole, and the other shall be just entrained or ejected by the outflow. It may be possible that the real efficiency could reach higher values (instead of  $10^{-2} - 10^{-3}$  adopted in our successful simulations).

For example, follow this consideration and let us define the inflow rate as the sum of the real BH accretion rate and the gas outflow rate:  $\dot{M}_{\text{in}} \equiv \dot{M}_{\text{acc}} + \dot{M}_{\text{out}}$ . If  $\eta \equiv \dot{M}_{\text{out}}/\dot{M}_{\text{acc}}$ , then the jet power  $P_{\text{jet}} \equiv \epsilon_{\text{real}} \dot{M}_{\text{acc}} c^2 = \epsilon_{\text{real}} \dot{M}_{\text{in}} c^2 / (1 + \eta)$ . Thus we can say that the mechanical efficiency adopted in our simulations could be  $\epsilon = \epsilon_{\text{real}} / (1 + \eta)$ . A mean  $\eta$  can be retrieved as  $\Delta M_{\text{in}} / \Delta M_{\text{acc}} - 1$ . Now, assuming a small BH mass variation in 7 Gyr of  $0.1 M_{\text{BH}}$  (that is  $\Delta M_{\text{acc}} \simeq 3 \times 10^8 M_{\odot}$ ), and noting that for model A3  $\Delta M_{\text{in}} = \Delta M_{\text{cold}} \simeq 3 \times 10^9 M_{\odot}$ , then clearly  $\eta \sim 9$ . With this in mind, the real efficiency may be  $\epsilon_{\text{real}} = (1 + \eta)\epsilon \sim 10\epsilon = 5 \times 10^{-2}$ . Not only, we can also estimate  $\Delta M_{\text{out}} \simeq 2.7 \times 10^9 M_{\odot}$  and, with a duty cycle of 10%, the mean outflow rate results in a few  $M_{\odot} \text{ yr}^{-1}$ . From here we can check the entrainment (or ‘mass loading’):  $\lambda_{\text{en}} = \dot{M}_{\text{act}}/\dot{M}_{\text{out}}$ , where  $\dot{M}_{\text{act}}$  is the outflow rate in the active region. Taking a mean value of  $10^3 M_{\odot} \text{ yr}^{-1}$ , the entrainment is  $\lambda_{\text{en}} \sim 10^2 - 10^3$ .

Summarizing, in order to have a small BH growth, in one of our best models, we have to assume massive outflows with a rate  $\sim 9$  times the accretion one. The ratio  $\eta$  is not well constrained, but for example Moe et al. (2009) give values around 10. Nowadays nobody knows how much gas is really loaded by the original jet, but  $\sim 10^2 - 10^3$  seems reasonable (Cattaneo & Teyssier 2007 adopted 100 for ex-

ample). This could be in the future another observational constraint for our numerical models.

We conclude from all this reasoning that the high ‘accretion’ rates in our successful simulations can be easily reduced, introducing a higher (real) efficiency and considering that only a fraction of  $\Delta M_{\text{cold}}$  falls onto BH, while the other part is ejected and entrained.

The second flaw in models A may be that the process of cavity formation heats the surrounding ICM too much (Section 5.1): soon after jet ignition the temperature inside the bubble rises to high value ( $\sim 10^8$  K), and the ICM around is highly shocked. On the other side many observations (Fabian et al. 2000; McNamara et al. 2000; Blanton et al. 2001, 2003; Nulsen et al. 2002; Fabian et al. 2003, 2006; MN07) suggest that the bubble inflation should be gentler, in order to produce rims of gas cooler than the ambient medium. Again our resolution does not permit an accurate and detailed study of this and other kind of features (e.g. cold filaments). Certainly, a direct cause of the violent behaviour is that the injection energy in a single timestep is too much. This will probably be avoided with higher spatial resolution, because of smaller  $\Delta t$  and therefore smaller  $\Delta M_{\text{cold}}$  and blowing instant power. Unfortunately with current computational resources we were limited to a very short evolution. In any case we plan to develop such a study in a future work.

We can also argue that observations may be seeing bubbles at a late time, well after their generation, and this could explain lower temperature and SB jumps. In fact of the three cavities analysed in Fig. 13, just the newly born one present sharp contrasts, while the other are older and hence feebler. Moreover, we can not exclude that in the entire simulation some bubbles are created in a gentler way by weaker bursts ( $\sim 10^{46}$  erg  $\text{s}^{-1}$ ).

### 6.3 Hot-regulated gentle feedback (Bondi)

To circumvent some of the aforementioned difficulties encountered with feedback A method, we changed completely direction, calculating models where the accretion rate was set to the Bondi rate. Contrary to models A, this generates a continuous feedback of moderate power (typically few  $\times 10^{44}$  erg  $\text{s}^{-1}$ ). In order to be efficient, such non explosive jet power must be sufficiently steady in order to reduce cooling flow. As pointed out in Section 2.2, our resolution is far above Bondi radius ( $\sim 50$  pc), thus we have to rely again upon mean large scale quantities. In this case we must stay as much possible close to the BH, avoiding the simplest case of a few cells, because of numerical fluctuations. When the radius of  $(\rho, c_s)$  averaging is fairly small,  $\sim 5$  kpc, the power is steady and the model successful: cooling rate are low, profiles follow observations, and energies are contained.

On the other side, with  $r_{\text{av}} \sim 10$  kpc, we revert again to a spasmodic feedback very sensitive to central cold mass. Hence this Bondi model recalls low efficiency A1 model. This behaviour is also emphasized by the fact that here we are injecting mechanical energy directly in the domain cells, and not through a boundary (like BOND12). In a short bursting event like models A this difference is not relevant, while with a continuous outflow, pushing the gas from below and not changing suddenly internal flow variables, seem to be a more efficient way to heat the inflowing central medium.

This illustrates the (unfortunate) sensitivity of the simulations on some numerical detail. The cause is that any kind of AGN feedback simulation with large spatial and temporal scale integration must require a few quantities set by-hand. In general a fully self-consistent simulation is rather utopian, for now. In our case the ignorance of detailed AGN accretion and jet-outflow physics, plus today computational resources, limits us to simplified numerical feedback models. Nevertheless, after trying many possible models and different parameters, they let us study very well the consequences of this assumptions on scales of interest.

#### 6.3.1 Riddles

A flaw we found in successful Bondi models is that they do not naturally generate X-ray cavities. Instead, the continuous outflows carve a narrow and long tunnel along the  $z$ -axis. However, we have seen that continuous jets, with ram pressure almost equal to gas thermal pressure, are highly disrupted by turbulence, especially in central regions. Hence, the fragmentation of a feeble jet may produce generations of ‘gentle’ detached bubbles, which rise buoyantly, even in continuous feedback models.

We propose that any kind of strong turbulence can indeed disrupt a moderate power jet. For example, Morsony et al. (2010) tried to start with a cluster atmosphere in non hydrostatic equilibrium, i.e. following a real cosmological evolution (local density fluctuations, merging, etc.), and they found a fragmentation of the AGN jets, helping the deposition of energy in the inner core.

The creation of an unidirectional channel and subsequent energy deposition at too large radii was pointed out by Vernaleo & Reynolds (2006). However, if we perform long term evolutions, we have showed that the above mentioned turbulence and vorticity promotes mixing in the central active region, replenishing again the channel. Even in BOND12 model, where a small narrow channel always stays open, instabilities and turbulence clearly heat the gas at the base of the jet, letting to cool only a moderate amount of gas in the near equatorial region.

### 6.4 Best models confrontation

It is interesting to find other important differences (or similarities) in successful models A and Bondi. The latter displays low velocities of the order  $6 - 7 \times 10^3$  km  $\text{s}^{-1}$ , a value consistent with line-absorption observations (see Crenshaw et al. 2003 for a review, and other references in Section 1). Explosive models A tend to have also higher velocities, in a few events reaching  $\sim 10^5$  km  $\text{s}^{-1}$ , more similar to a fast jet than an outflow wind. Both models have reasonable final injected energies, below a theoretical total energy of a BH with mass  $10^9$ ,  $\sim 2 \times 10^{62}$  erg.

Apart from cavities and shocks (previously discussed), we produce other significant predictions, which are (or will be) comparable to X-ray observations. Iron abundance maps play a relevant role in tracing the outflow activity. The metals, produced mainly by SNIa in the cD elliptical galaxy, are easily transported along jet-axis up to 150-200 kpc, creating an unmistakable asymmetry, when the AGN is very active. The observations by Kirkpatrick et al. (2009) and Doria et

al. (prep.) confirm this behaviour. In the period of quiescence turbulence and bulk motion will dominate the scene, smoothing and almost restoring the homogeneity. This could be another constraint in choosing between Bondi or not: in fact a continuous jet will tend to show often this marked asymmetry.

Finally, another striking diversity is the clean departure from hydrostatic equilibrium in models A, due to its more explosive nature. On the contrary, in Bondi type, mean fluctuations are very contained with errors below 8%. The consequence is, in the first case, a less precise mass determination using Eq. (5), as also found by other observational works (Nagai et al. 2007; Rasia et al. 2006).

We conclude pointing out that the gaps of models A, can be replenished by the features of Bondi feedback, and viceversa (especially for cavities). Thus, an intriguing solution may be a ‘dual model’, in which few energetic AGN outbursts (like models A3-4), perhaps triggered by accretion rates close to the Eddington limit, are superimposed (or alternated) to the weak activity induced by Bondi prescription. The first explosive mode will create large spheroidal bubbles, as those observed in real clusters, while the second quasi-steady outflow will be the real sustaining pillar of the heating machine. This scenario would require a physical explanation of the alternation mechanism or why the two types of outflow are diversified.

## 7 CONCLUSIONS

Overall we found that subrelativistic AGN outflows, produced by two types of self-regulated feedback, are able to quench cooling flow for at least 7 Gyr and, at the same time, preserve the cool core appearance:

(a) self-regulated feedback based on the instantaneous  $\Delta M_{\text{cool}}$  accreted, with mechanical efficiencies between  $\sim 5 \times 10^{-3} - 10^{-2}$ ;

(b) Bondi triggered feedback with  $\epsilon$  around 0.1, based on an almost continuous and steady outflow, generated by hot gas accretion.

Both best models (a) and (b) present primary merits concordant with X-ray observations:

(1a, b) cooling rate is reduced at least under 5% of the pure CF model;

(2a, b) (mass-weighted)  $T(r)$  and  $n(r)$  profiles oscillate near the observed ones;

(3a, b) total injected energy is always below  $2 \times 10^{62}$  erg, under the limit of  $E_{\text{BH}}$ ;

(4a, b) mean  $v_{\text{jet}}$ : from  $\sim 5 \times 10^3$  to a few  $10^4$  km s $^{-1}$ .

Intermittent (B) or continuous scheme with fixed velocity (C) are not consistent in the long term with some of these points, and hence rejected.

In addition to these constraints we wanted to test further the best models. We warn that the following are supple-

mentary predictions, but not main goals of our study: due to the need of a long term evolution, our simulations are limited in resolution ( $\sim$  kpc), and fine details could be altered or just missed by our numerical implementation. Marked differences between the two best models are:

(5a) super-Eddington  $\dot{M}_{\text{acc}}$ : high power ( $\sim 10^{48}$  erg s $^{-1}$ );

(5b) sub-Eddington  $\dot{M}_{\text{acc}}$ : low power ( $\sim 10^{44}$  erg s $^{-1}$ );

(6a) cavities with high internal energy and shocked rims;

(6b) absence of a duty cycle and real inflated bubbles;

(7a) asymmetrical transport of metals (SNIa) along jet-axis up to 200 kpc; subsequent gradient lengthened by turbulence;

(7b) almost always asymmetrical iron maps;

(8a) large deviation from hydrostatic equilibrium state (high turbulence);

(8b) deviation from HE mass determination below 8% (moderate turbulence).

Points (6) (caused by (5)) seem not to follow entirely observations (even if we need larger samples of clusters with AGN activity to reconstruct global history, and certainly higher resolved SB maps to study cavities). While the two models appear at first sight antithetical, it might be possible that they alternate during evolution, or that high power outbursts are just superimposed to a low Bondi feedback.

Despite these riddles, purely mechanical AGN outflows promise to be good candidates, to uphold the wild and frenetic ‘dance’ between heating and cooling.

## ACKNOWLEDGMENTS

The software used in this work was in part developed by the DOE supported ASCI/Alliances Centre for Thermonuclear Flashes at the University of Chicago. We acknowledge the CINECA-INAF 2008-2010 agreement for the availability of high performance computing resources, and the support by MIUR grant PRIN 2007C53X.

## REFERENCES

- Allen S.W., Dunn R.J.H., Fabian A.C., Taylor G.B., Reynolds C.S., 2006, MNRAS, 372, 21
- Baldi A., Forman W., Jones C., Kraft R., Nulsen P., Churazov E., David L., Giacintucci S., 2009, ApJ, 707, 1034
- Basson J.F., Alexander P., 2003, MNRAS, 339, 353
- Blanton E.L., Sarazin C.L., McNamara B.R., Wise M.W., 2001, ApJ, 585, 227
- Blanton E., Sarazin C.L., McNamara B.R., 2003, ApJ, 585, 227
- Blanton E., Randall S.W., Douglass E.M., Sarazin C.L., Clarke T.E., McNamara B.R., 2009, ApJ, 697, L95
- Bondi H., 1952, MNRAS, 112, 195

- Boehringer H., Voges W., Fabian A.C., Edge A.C., Neumann D.M., 1993, MNRAS, 264, L25
- Bregman J.N., Fabian A.C., Miller E.D., Irwin J.A., 2006, ApJ, 642, 746
- Brighenti F., Mathews W.G., 2000, ApJ, 535, 650
- Brighenti F., Mathews W.G., 2002, ApJ, 567, 130
- Brighenti F., Mathews W.G., 2003, ApJ, 587, 580
- Brighenti F., Mathews W.G., 2006, ApJ, 643, 120 [BM06]
- Brueggen M., Kaiser C.R., 2002, Nature, 418, 301
- Brueggen M., Scannapieco E., 2009, MNRAS, 398, 548
- Brueggen M., Ruszkowski M., Hallman E., 2005, ApJ, 630, 740
- Brueggen M., Heinz S., Roediger E., Ruszkowski M., Simionescu A., 2007, MNRAS, 380, L67
- Buote D.A., Tsai J.C., 1996, ApJ, 458, 27
- Buote D. A., Gastaldello F., Humphrey P. J., Zappacosta L., Bullock J. S., Brighenti F., Mathews W. G., 2007, ApJ, 664, 123
- Capellaro E., Evans R., Turatto M., 1999, A&A, 351, 45
- Cattaneo A., Teyssier R., 2007, MNRAS, 376, 1547
- Cattaneo A., Faber S.M., Binney J., et al., 2009, Nature, 460, 213
- Crenshaw D.M., Kraemer S.B., Boggess A., et al., 1999, ApJ, 516, 750
- Crenshaw D.M., Kraemer S.B., George I.M., 2003, ARAA, 41, 117
- Dunn R.J.H., Fabian A.C., Taylor G.B., 2005, MNRAS, 364, 1343
- Dalla Vecchia C., Bower R.G., Theuns T., Balogh M.L., Mazzotta P., Frenk C.S., 2004, MNRAS, 355, 995
- Ettori S., Brighenti F., 2008, MNRAS, 387, 631
- Ettori S., Fabian A.C., Allen S.W., Johnstone R.M., 2002, MNRAS, 331, 635
- Fabian A.C., 1994, ARAA, 32, 277
- Fabian A.C., 2009, in Peterson B.M., Somerville R.S., Storchi-Bergmann T., eds., Proceedings IAU Symposium No. 267, ‘Co-Evolution of Central Black Holes and Galaxies’
- Fabian A.C., Sanders J.S., Ettori S., et al., 2000, MNRAS, 318, L65
- Fabian A.C., Sanders J.S., Crawford C.S., Conselice C.J., Gallagher J.S., Wyse, R.F.G., 2003, MNRAS, 344, L48
- Fabian A.C., Sanders J.S., Taylor G.B., Allen S.W., Crawford C.S., Johnstone R.M., Iwasawa K., 2006, MNRAS, 366, 417
- Finoguenov A., Jones C., 2001, ApJ, 557, L107
- Fryxell B., Olson K., Ricker P., et al., 2000, ApJS, 131, 273
- Gardini A., 2007, A&A, 464, 143
- Gardini A., Rasia E., Mazzotta P., Tormen G., De Grandi S., Moscardini L., 2004, MNRAS, 351, 505
- George I.M., Turner T.J., Netzer H., Nandra K., Mushotzky R.F., Yaqoob T., 1998, ApJS, 114, 73
- Ghosh S., Mukhopadhyay B., Krishan V., Khan M., 2010, NewA, 15, 83
- Gitti M., O’Sullivan E., Giacintucci S., David L. P., Vrtilick J. M., Raychaudhury S., Nulsen, P. E. J., 2009, preprint (astro-ph/0912.3013)
- Giovannini G., 2004, Ap&SS, 293, 1
- Greggio L., 2005, A&A, 441, 1055
- Guo F., Mathews W.G., 2010, ApJ, 712, 1311
- Hatch N.A., Crawford C.S., Johnstone R.M., Fabian A.C., 2006, MNRAS, 367, 433
- Heinz S., Brueggen M., 2009, preprint (astro-ph/0903.0043)
- Heinz S., Brueggen M., Young A., Levesque E., 2006, MNRAS, 373, L65
- Hopkins P.F., Narayan R., Hernquist L., 2006, ApJ, 643, 641
- Humphrey P.J., Buote D.A., 2006, ApJ, 639, 136
- Jones C., Forman W., Vikhlinin A., Markevitch M., David L., Warmflash A., Murray S., Nulsen P. E. J., 2002, ApJ, 567, L115
- King A.R., 2009, MNRAS, 402, 1516
- Kirkpatrick C.C., Gitti M., Cavagnolo K.W., McNamara B.R., David L.P., Nulsen P.E.J., Wise M.W., 2009, ApJ, 707, L69
- Kriss G.A., 2003, A&A, 403, 473
- La Franca F., Melini G., Fiore F., 2010, preprint (astro-ph/1006.1247)
- Mathews W.G., 2009, ApJ, 695, 128
- Mathews W.G., Brighenti F., 2003
- Mathews W.G., Brighenti F., 2008a, ApJ, 676, 880
- Mathews W.G., Brighenti F., 2008b, ApJ, 685, 128
- Mathews W.G., Faltenbacher A., Brighenti F., 2006, ApJ, 638, 659
- McKernan B., Yaqoob T., Reynolds C.S., 2007, MNRAS, 379, 1359
- Mcnamara B.R., Nulsen P.E.J., 2007, ARAA, 45, 117 [MN07]
- McNamara B.R., Wise M., Nulsen P.E.J., 2000, ApJ, 534, L135
- Mellier Y., Mathez J., 1987, A&A, 175, 1
- Merloni A., Heinz S., 2008, MNRAS, 388, 1011
- Mittal R., Hudson D.S., Reiprich T.H., Clarke T., 2009, A&A, 501, 850
- Moe M., Arav N., Bautista M.A., Korista K.T., 2009, ApJ, 706, 525
- Morganti R., Tadhunter C.N., Oosterloo T., 2005, A&A, 444, L9
- Morganti R., Holt J., Saripalli L., Oosterloo T., Tadhunter C.N., 2007, A&A, 476, 735
- Morsony B.J., Heinz S., Brueggen M., Ruszkowski M., 2010, preprint (astro-ph/1003.3049)
- Nagai D., Vikhlinin A., Kravtsov A.V., 2007, ApJ, 655, 98
- Navarro J.F., Frenk C.S., White S.D.M., 1996, ApJ, 462, 563
- Nesvadba N.P.H., Lehnert M.D., De Breuck C., Gilbert A.M., van Breugel W., 2008, A&A, 491, 407
- Nulsen P.E.J., David L.P., McNamara B.R., 2002, ApJ, 568, 163
- Omma H., Binney J., Bryan G., Slyz A., 2004, MNRAS, 348, 1105
- Ostriker P. O., Choi E., Ciotti L., Novak G. S., Proga D., 2010, preprint (astro-ph:1004.2923)
- Peres C. B., Fabian A. C., Edge A. C., Allen S. W., Johnstone R. M., White D. A., 1998, MNRAS 298, 416
- Peterson J.R., Fabian A.C., 2006, Phis. Rep., 427, 1
- Peterson J.R., Paerels F.B.S., Kaastra J.S., et al., 2001, A&A, 365, L104
- Peterson J.R., Kahn S.M., Paerels F.B.S., Kaastra J.S., Tamura T., et al., 2003, ApJ, 590, 207
- Pounds K.A., Reeves J.N., 2009, MNRAS, 397, 249
- Proga D., 2007, in Ho L.C., Wang J.W., eds., ASP Conference Series Vol. 373, ‘The central engine of AGN’

- Rafferty D.A., McNamara B.R., Nulsen P.E.J., Wise M.W., 2006, *ApJ*, 652, 216
- Rafferty D.A., McNamara B.R., Nulsen P.E.J., 2008, *MNRAS*, 687, 899
- Rasia E., Ettori S., Moscardini L., et al., 2006, *MNRAS*, 369, 201
- Rasia E., Mazzotta P., Bourdin H., Borgani S., Tornatore L., Ettori S., Dolag K., Moscardini L., 2008, *ApJ*, 674, 728
- Reynolds C.S., Heinz S., Begelman M.C., 2001, *ApJ*, 549, L179
- Reynolds C.S., Heinz S., Begelman M.C., 2002, *MNRAS*, 332, 271
- Risaliti G., Bianchi S., Matt G., Baldi A., Elvis M., Fabiano G., Zezas A., 2005, *ApJ*, 630, L129
- Ruszkowski M., Brueggen M., Begelman M.C., 2004, *ApJ*, 611, 158
- Sanders J.S., Fabian A.C., 2007, *MNRAS*, 387, 1381
- Sanders J.S., Fabian A.C., 2008, *MNRAS*, 390, L93
- Sanderson A.J.R., Ponman T.J., O'Sullivan E., 2006, *MNRAS*, 372, 1496
- Sijacki D., Springel V., Di Matteo T., Hernquist L., 2007, *MNRAS*, 380, 877
- Sternberg A., Soker N., 2009, *MNRAS*, 395, 228
- Sternberg A., Pizzolato F., Soker N., 2007, *ApJ*, 656, L5
- Sun M., 2009, *ApJ*, 704, 1586
- Sun M., Vikhlinin A., Forman W., Jones C., Murray S.S., 2005, *ApJ*, 619, 169
- Sun M., Jones C., Forman W., Vikhlinin A., Donahue M., Voit M., 2007, *ApJ*, 657, 197
- Sutherland R. S., Dopita M. A., 1993, *ApJS*, 88, 253
- Szuskiewcz E., 2004, in Ho L.C., ed., *Carnegie Observatories Astrophysics Series Vol. 1, 'Coevolution of Black Holes and Galaxies'*
- Tamura T., Kaastra J.S., Peterson J.R., et al., 2001, *A&A*, 365, L87
- Tamura T., Kaastra J.S., den Herder J.W.A., Bleeker J.A.M., Peterson J.R., 2004, *A&A*, 420, 135-146
- Vernaleo J.C., Reynolds C.S., 2006, *ApJ*, 645, 83
- Vikhlinin A., Kravtsov A., Forman W., Jones C., Markevitch M., Murray S. S., Van Speybroeck, L., 2006, *ApJ*, 640, 691
- Wise M.W., McNamara B.R., Nulsen P.E.J., Houck J.C., David L.P., 2007, *ApJ*, 659, 1153
- Xu H., Kahn S.M., Peterson J.R., et al., 2002, *ApJ*, 579, 600
- Zanni C., Murante G., Bodo G., Massaglia S., Rossi P., Ferrari A., 2005, *A&A*, 429, 399

This paper has been typeset from a  $\text{\TeX}$ / $\text{\LaTeX}$  file prepared by the author.